

AERO. & ASTRO. LIBRARY



FR 12/6

# NATIONAL ADVISORY COMMITTEE FOR AERONAUTICS

REPORT 1216

*Copy # 3*

## CHARTS FOR ESTIMATING TAIL-ROTOR CONTRIBUTION TO HELICOPTER DIRECTIONAL STABILITY AND CONTROL IN LOW-SPEED FLIGHT

By KENNETH B. AMER and ALFRED GESSOW



623-742  
6582

1955

---

## **REPORT 1216**

---

# **CHARTS FOR ESTIMATING TAIL-ROTOR CONTRIBUTION TO HELICOPTER DIRECTIONAL STABILITY AND CONTROL IN LOW-SPEED FLIGHT**

By **KENNETH B. AMER** and **ALFRED GESSOW**

**Langley Aeronautical Laboratory  
Langley Field, Va.**

---

# National Advisory Committee for Aeronautics

*Headquarters, 1512 H Street NW., Washington 25, D. C.*

Created by act of Congress approved March 3, 1915, for the supervision and direction of the scientific study of the problems of flight (U. S. Code, title 50, sec. 151). Its membership was increased from 12 to 15 by act approved March 2, 1929, and to 17 by act approved May 25, 1948. The members are appointed by the President, and serve as such without compensation.

JEROME C. HUNSAKER, Sc. D., Massachusetts Institute of Technology, *Chairman*

LEONARD CARMICHAEL, Ph. D., Secretary, Smithsonian Institution, *Vice Chairman*

JOSEPH P. ADAMS, LL. B., Vice Chairman, Civil Aeronautics Board.  
ALLEN V. ASTIN, Ph. D., Director, National Bureau of Standards.  
PRESTON R. BASSETT, M. A., Vice President, Sperry Rand Corp.  
DETLEV W. BRONK, Ph. D., President, Rockefeller Institute for Medical Research.  
THOMAS S. COMBS, Vice Admiral, United States Navy, Deputy Chief of Naval Operations (Air).  
FREDERICK C. CRAWFORD, Sc. D., Chairman of the Board, Thompson Products, Inc.  
RALPH S. DAMON, D. Eng., President, Trans World Airlines, Inc.  
JAMES H. DOOLITTLE, Sc. D., Vice President, Shell Oil Co.  
CARL J. PFINGSTAG, Rear Admiral, United States Navy, Assistant Chief for Field Activities, Bureau of Aeronautics.

DONALD L. PUTT, Lieutenant General, United States Air Force, Deputy Chief of Staff (Development).  
DONALD A. QUARLES, D. Eng., Secretary of the Air Force.  
ARTHUR E. RAYMOND, Sc. D., Vice President—Engineering, Douglas Aircraft Co., Inc.  
FRANCIS W. REICHELDERFER, Sc. D., Chief, United States Weather Bureau.  
LOUIS S. ROTHSCHILD, Ph. B., Under Secretary of Commerce for Transportation.  
NATHAN F. TWINING, General, United States Air Force, Chief of Staff.

---

HUGH L. DRYDEN, Ph. D., *Director*

JOHN W. CROWLEY, JR., B. S., *Associate Director for Research*

JOHN F. VICTORY, LL. D., *Executive Secretary*

EDWARD H. CHAMBERLIN, *Executive Officer*

---

HENRY J. E. REID, D. Eng., Director, Langley Aeronautical Laboratory, Langley Field, Va.

SMITH J. DEFANCE, D. Eng., Director, Ames Aeronautical Laboratory, Moffett Field, Calif.

EDWARD R. SHARP, Sc. D., Director, Lewis Flight Propulsion Laboratory, Cleveland, Ohio

WALTER C. WILLIAMS, B. S., Chief, High-Speed Flight Station, Edwards, Calif.

## REPORT 1216

# CHARTS FOR ESTIMATING TAIL-ROTOR CONTRIBUTION TO HELICOPTER DIRECTIONAL STABILITY AND CONTROL IN LOW-SPEED FLIGHT<sup>1</sup>

By KENNETH B. AMER and ALFRED GESSOW

### SUMMARY

*Theoretically derived charts and equations are presented by which tail-rotor design studies of directional trim and control response at low forward speed can be conveniently made. The charts can also be used to obtain the main-rotor stability derivatives of thrust with respect to collective pitch and angle of attack at low forward speeds.*

*The use of the charts and equations for tail-rotor design studies is illustrated. Comparisons between theoretical and experimental results are presented.*

*The charts indicate, and flight tests confirm, that the region of vortex roughness which is familiar for the main rotor is also encountered by the tail rotor and that prolonged operation at the corresponding flight conditions would be difficult.*

### INTRODUCTION

The tail rotor of a conventionally powered single-rotor helicopter has two purposes—to counteract the rotor torque and fuselage yawing moments and to maneuver the helicopter directionally. Preliminary flying-quality studies have indicated a minimum desirable response of 3° yaw in the first second following a 1-inch step displacement of the pedals while hovering in zero wind. In addition to indicating a minimum desirable response value, these studies have also indicated the existence of a maximum desirable response value. When large pedal friction and out-of-trim forces are present, the maximum desirable response value is indicated to be approximately 10° of yaw in the first second following a 1-inch step displacement of the pedals while hovering in zero wind. When pedal friction and out-of-trim forces are relatively small, a maximum desirable value of 2 to 4 times as large as the 10° value is indicated.

Some of these flying-quality indications are incorporated in the flying-quality requirements of reference 1. In addition, reference 1 calls for the ability of average-sized helicopters to make a complete turn over a spot while hovering in a 30-knot wind and, while trimmed at the most critical yaw angle, to be able to achieve at least 3° of yaw in the first second following full deflection of the pedals in the critical direction. Other flying-quality and stability studies have indicated that careful design is frequently required to satisfy these criteria without unnecessary sacrifice in weight, rotor clearances, or other factors. Tail rotors for jet-powered helicopters, for example, are of minimum size inasmuch as their primary purpose is to pro-

vide control and, unless specifically designed to satisfy the previously discussed requirements, might not fulfill all of these criteria.

As an aid in designing helicopters to meet the directional requirements of reference 1, it would, of course, be desirable to have published information whereby problems of directional trim and control can be conveniently studied for helicopters of various types and configurations. The single-rotor helicopter was chosen for study in this report because of its wide usage and because the necessary background theory is readily available. The results of the study are presented in the form of charts and related equations, and a comparison is made between theoretical and experimental results. In the course of this comparison, a region of possible directional-control difficulty is indicated.

The charts presented herein can also be used to obtain the main-rotor stability derivatives relating the change in thrust-coefficient—solidity ratio with pitch angle  $\frac{\partial C_T/\sigma}{\partial \theta}$  and with angle of attack  $\frac{\partial C_T/\sigma}{\partial \alpha}$  at low forward speeds (at tip-speed ratios less than 0.10). The significance of these derivatives is discussed in reference 2, which also presents charts for obtaining them for tip-speed ratios equal to or greater than 0.15.

### SYMBOLS

- |       |  |
|-------|--|
| $a$   | slope of curve of section lift coefficient against section angle of attack in radians (assumed herein to be 5.73)                |
| $b$   | number of blades per rotor   |
| $B$   | tip-loss factor (assumed herein to be 0.97); blade elements outboard of radius $BR$ are assumed to have profile drag but no lift |
| $c$   | blade section chord, ft  |
| $c_e$ | equivalent blade chord (on thrust basis), $\frac{\int_0^{1.0} cx^2 dx}{\int_0^{1.0} x^2 dx}$ , ft                                |
| $C_T$ | thrust coefficient, $\frac{T}{\pi R^2 \rho (\Omega R)^2}$  |
| $C_Q$ | rotor-shaft torque coefficient, $\frac{Q}{\pi R^2 \rho (\Omega R)^2 R}$  |
| $I_Z$ | mass moment of inertia, referenced to Z-axis (vertical axis through center of gravity), slug-ft <sup>2</sup>                     |

<sup>1</sup> Supersedes NACA TN 3156, 1954.

$l_t$	horizontal distance from tail-rotor hub to main-rotor hub, ft
$N$	yawing moment, lb-ft
$Q$	rotor-shaft torque, lb-ft
$r$	rate of yaw with respect to earth axes, $\frac{d\eta}{dt}$ , radians/sec
$R$	blade radius, ft
$s$	Laplace transform parameter
$P$	rotor-shaft power, hp
$T$	rotor thrust, lb
$t$	time, sec
$v$	induced inflow velocity at rotor (always positive), ft/sec
$V$	true airspeed of helicopter along flight path, ft/sec
$x$	ratio of blade-element radius to rotor-blade radius
$\alpha$	rotor angle of attack (angle between flight path and plane perpendicular to axis of no feathering, positive when axis is inclined rearward), radians
$\alpha_{\frac{2}{3}BR}$	blade-element angle of attack at radial position $\frac{2}{3}BR$ (measured from line of zero lift), deg
$\beta$	sideslip angle (angle between plane of symmetry and flight path, positive for sideslip to right); for tail-rotor thrust to right, $\beta_t = -\alpha_t$ , radians
$\delta_r$	"rudder" pedal deflection, positive for right pedal forward, in.
$\eta$	angle of yaw with respect to earth axes, radians
$\theta$	blade-section pitch angle (angle between line of zero lift of blade section and plane perpendicular to axis of no feathering), radians unless otherwise stated
$\theta_0$	blade pitch angle at hub, radians
$\theta_1$	difference between hub and tip pitch angles, positive when tip angle is larger, radians
$\lambda$	inflow ratio, $(V \sin \alpha - v)/\Omega R$
$\mu$	tip-speed ratio, $V \cos \alpha/\Omega R$
$\rho$	mass density of air, slugs/cu ft
$\sigma$	rotor solidity, $bc_e/\pi R$
$\Omega$	rotor angular velocity with respect to helicopter, positive in counterclockwise direction as viewed from above, radians/sec

## Subscripts:

$hov$	hovering
$i$	induced
$m$	main rotor
$BR$	at radial position $BR$
$t$	tail rotor; this subscript is used only where there might be some confusion as to which rotor is being discussed

## ANALYSIS

Problems of directional trim and control response of the single-rotor helicopter involve a knowledge of the relation between tail-rotor collective pitch and various operating and design variables as well as an understanding of the dynamic response of the helicopter to control deflection. Both types of information are discussed in this section.

## STATIC ROTOR CHARACTERISTICS

Tail-rotor collective-pitch relations can be most conveniently studied by means of charts that are presented herein. The theory on which the charts are based is developed in appendix A, and the application of the charts is illustrated in the section entitled "Illustrative Calculations."

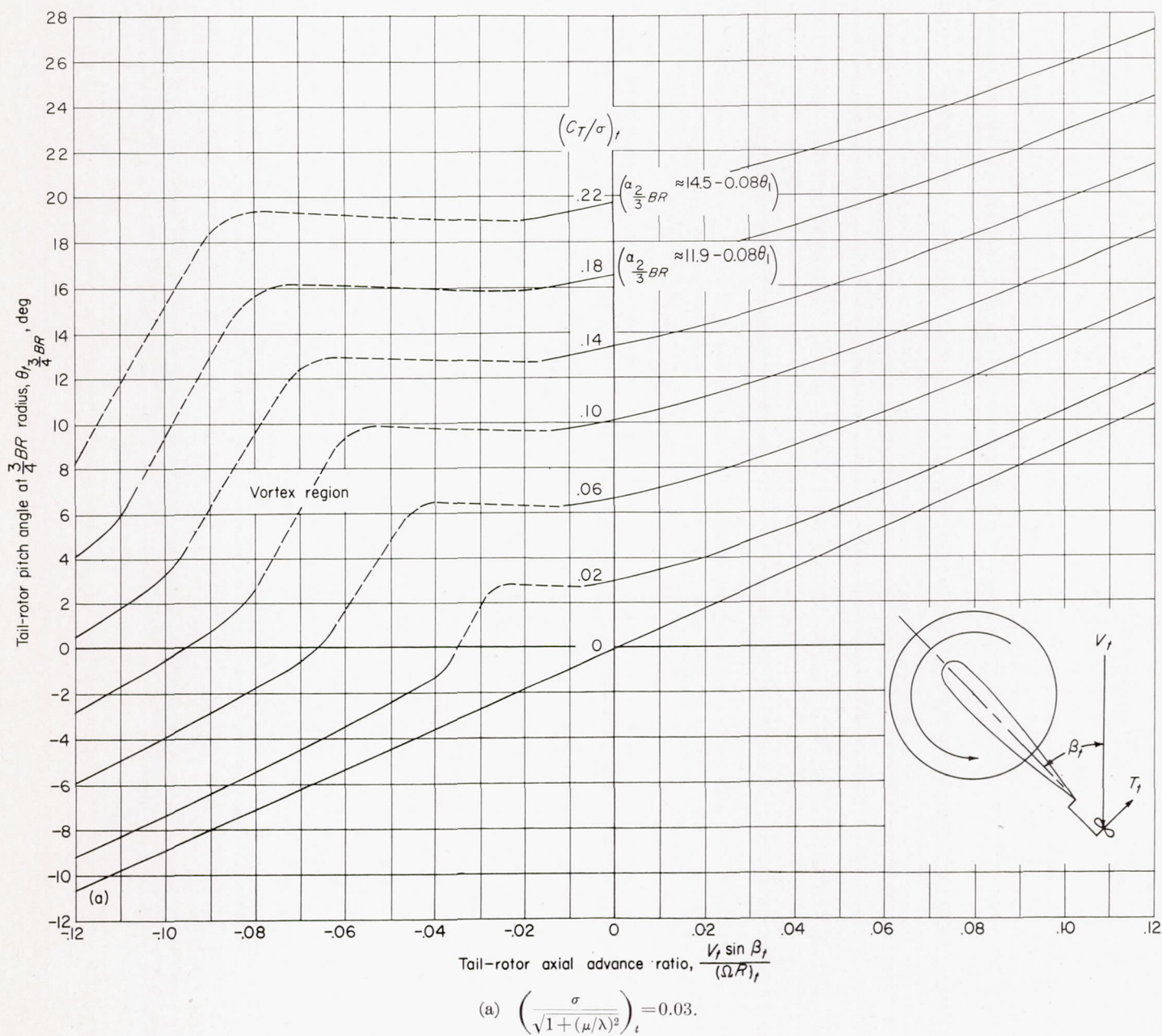
In appendix A, equations for the collective pitch of a tail rotor at low forward speeds are derived in terms of its forward speed, tip speed, sideslip angle, thrust coefficient, solidity, and the yawing velocity of the helicopter. The derivations are based on the rotor theory of references 3 and 4. The assumptions involved are discussed in appendix A. Comparison of the equations with more accurate but less general calculations presented in references 5 and 6 is made in appendix A and shows good agreement. The charts based on the equations of appendix A are considered applicable to tip-speed ratios equal to or less than 0.10.

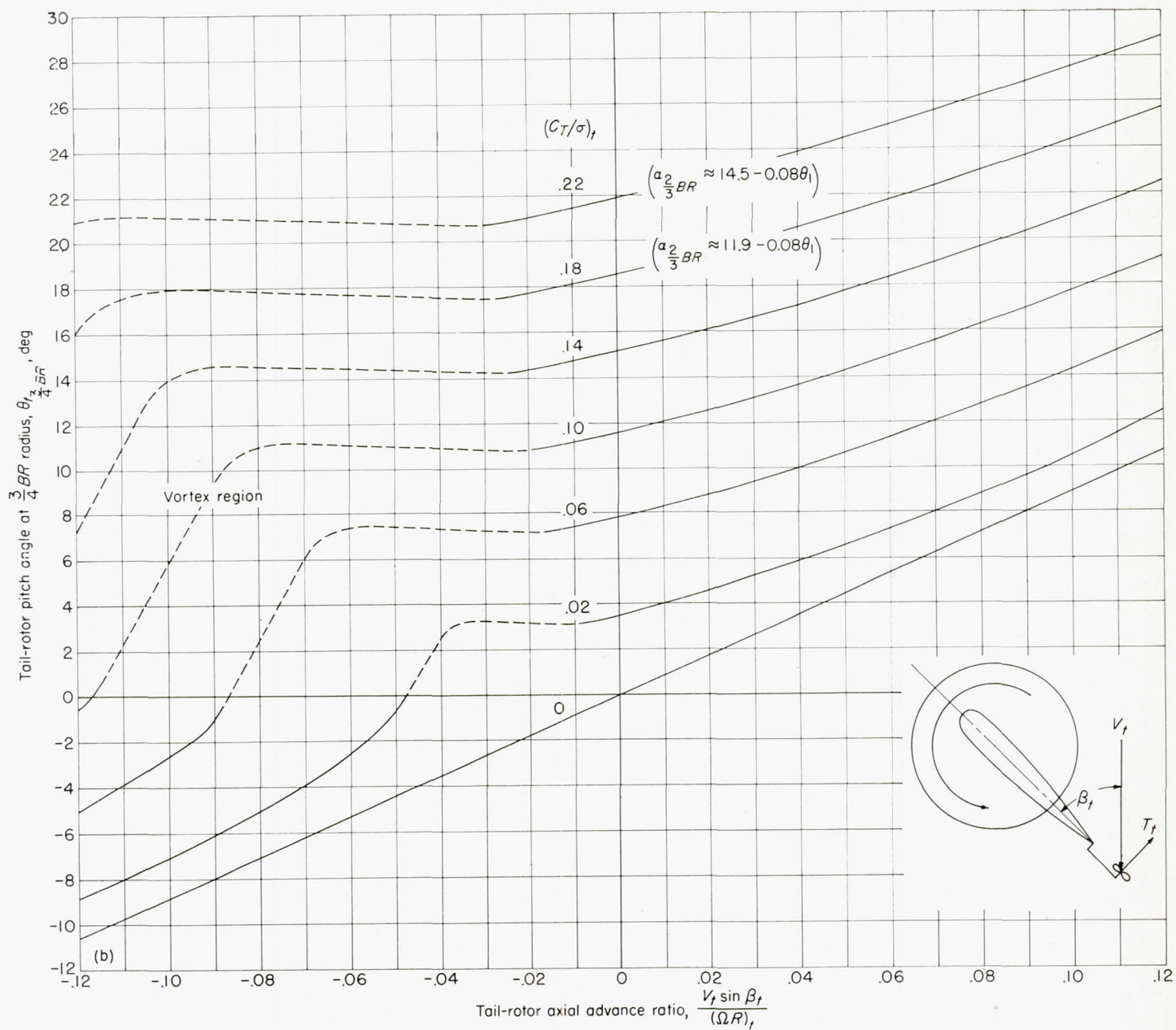
An expression is also derived in appendix A for determining typical blade-section angles of attack in the hovering or vertical-flight condition. This expression provides a basis for determining the limits of validity of the equations for tail-rotor collective pitch caused by tail-rotor stall. Another condition of operation wherein the theory becomes invalid is the vortex region. This region of operation is treated by means of a semiempirical theory and is also discussed in appendix A.

In figure 1,  $\theta_{\frac{3}{4}BR}$  (tail-rotor collective pitch angle at  $\frac{3}{4}BR$ ) is shown as a function of the axial advance ratio  $\left(\frac{V \sin \beta}{\Omega R}\right)_t$  for constant values of  $\left(\frac{C_T}{\sigma}\right)_t$  for  $\left(\frac{\sigma}{\sqrt{1+(\mu/\lambda)^2}}\right)_t = 0.03, 0.06, 0.09, \text{ and } 0.12$ . In the construction of figure 1, equations (A5) and (A6) were used for the region where the momentum theory was applicable. For the vortex region, figure 2 and equation (A1) were used as discussed in appendix A. The vortex region, the limits of which are given by equations (A12) and (A13), is shown dashed in figures 1 and 2.

Equation (A9) indicates that a line of constant  $C_T/\sigma$  corresponds to a constant value of  $\alpha_{\frac{2}{3}BR}$ . Thus, the lines for the larger values of  $\left(\frac{C_T}{\sigma}\right)_t$  are also labeled in figures 1 and 2 with the values of  $\alpha_{\frac{2}{3}BR}$  in order to allow their use for studies of blade stall.

Of the three quantities of which  $\theta_{\frac{3}{4}BR}$  is a function in figure 1, only the parameter  $\left(\frac{1}{\sqrt{1+(\mu/\lambda)^2}}\right)_t$  is not known at the start. Determination of this quantity is facilitated by plotting it in figure 3 against the tail-rotor sideslip angle  $\beta_t$  for constant values of the tail-rotor forward-speed parameter  $\left(\frac{V/\Omega R}{\sqrt{C_T/2B^2}}\right)_t$ . The regions where the momentum theory is applicable were obtained by iterative solution of equations

FIGURE 1.—Charts for determining  $\theta_{t, \frac{3}{4}BR}$ .



(b)  $\left( \frac{\sigma^2}{\sqrt{1 + (\mu/\lambda)^2}} \right)_t = 0.06.$

FIGURE 1.—Continued.

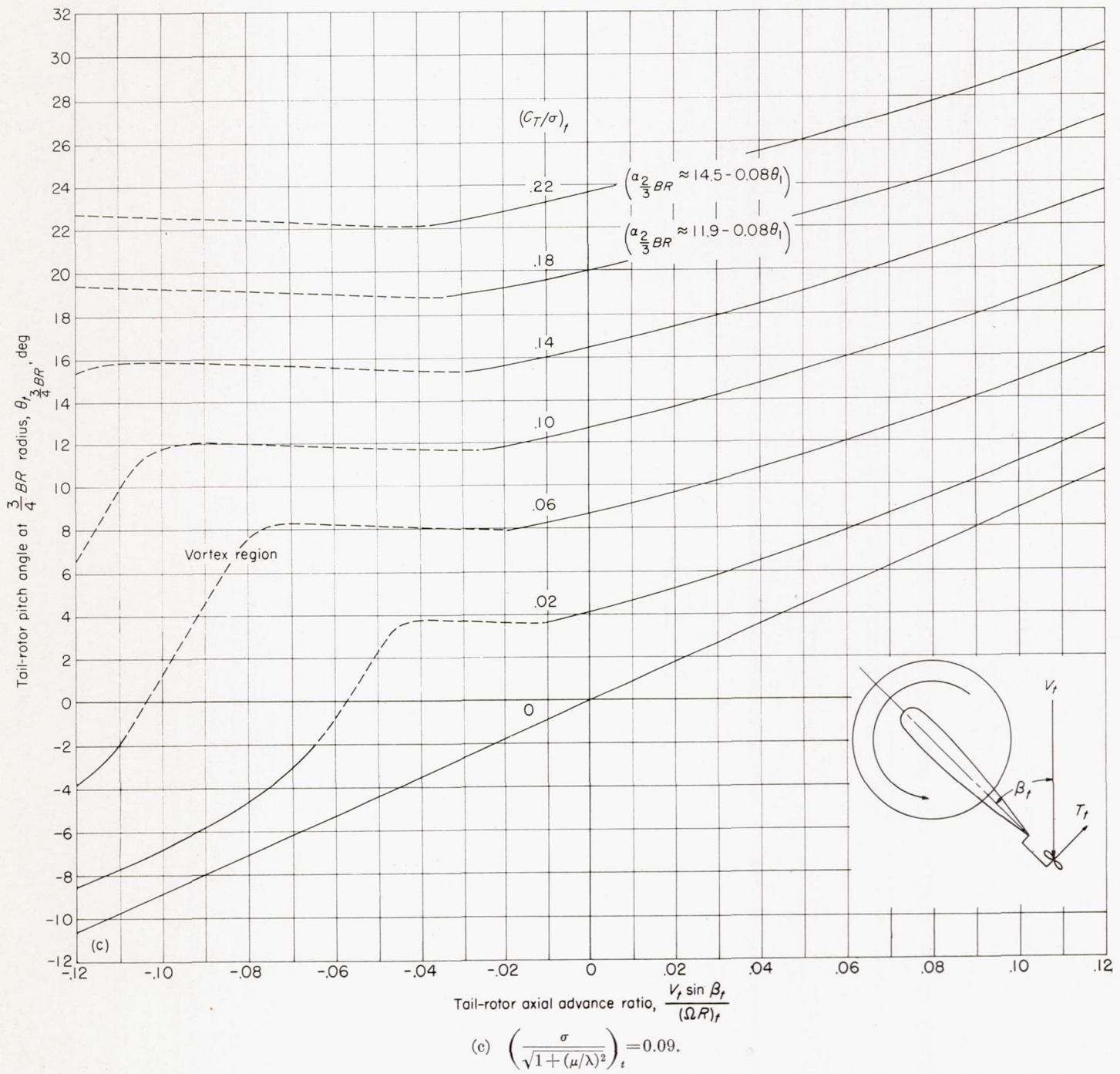
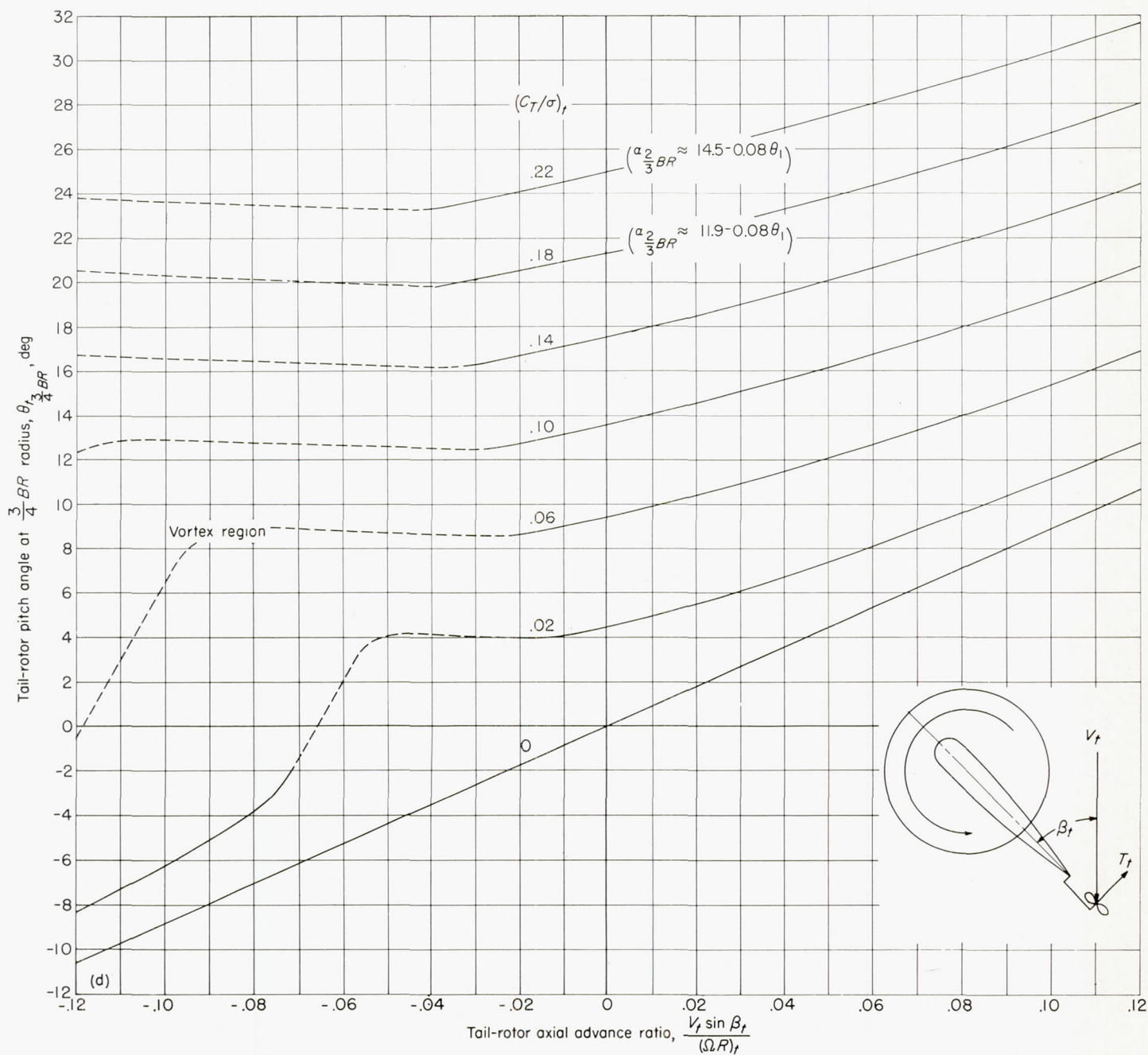


FIGURE 1.—Continued.



(d)  $\left(\frac{\sigma}{\sqrt{1 + (\mu/\lambda)^2}}\right)_t = 0.12.$

FIGURE 1.—Concluded.

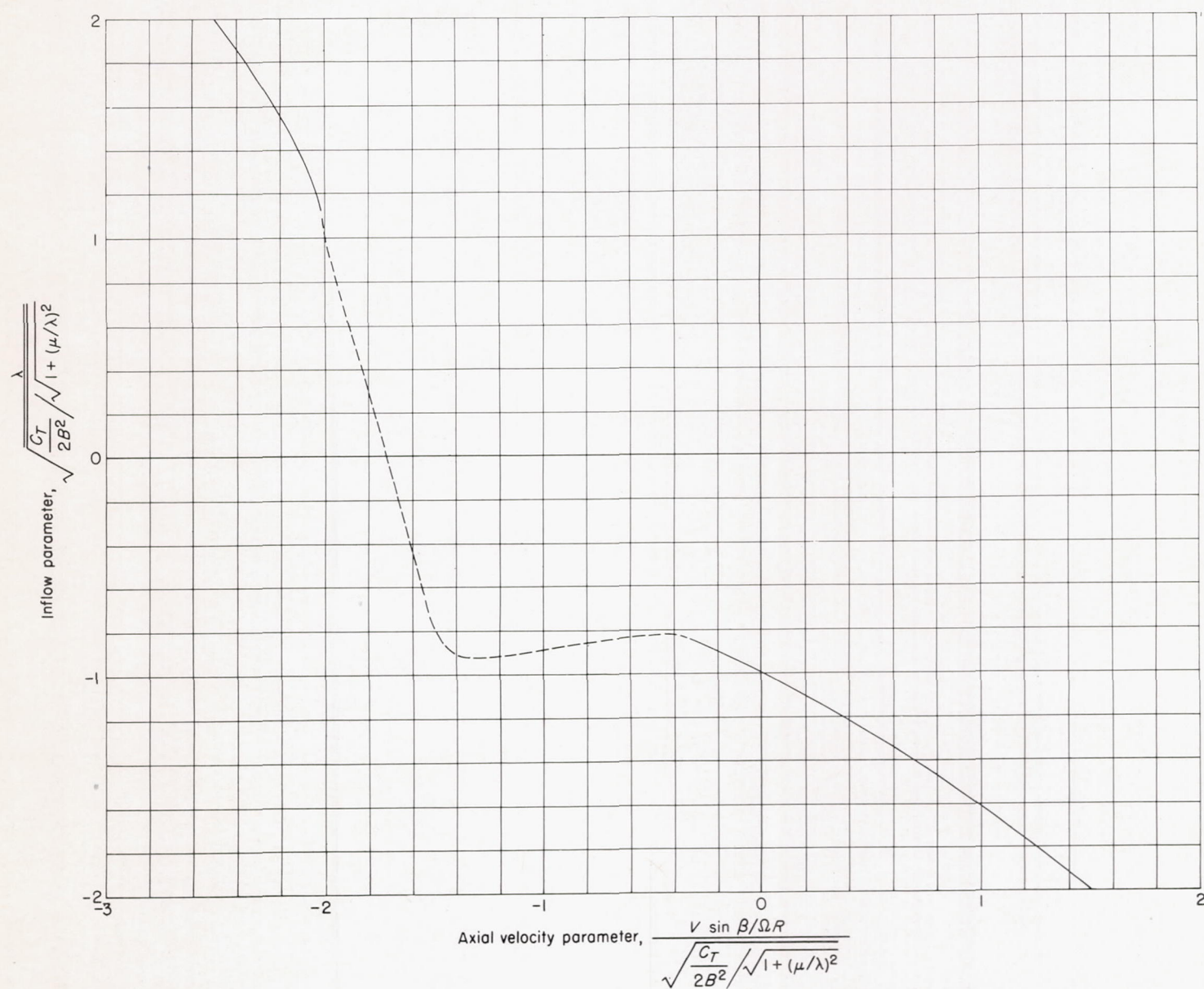


FIGURE 2.—Relation between inflow parameter and axial velocity parameter used in this report. Dashed line indicates vortex region.

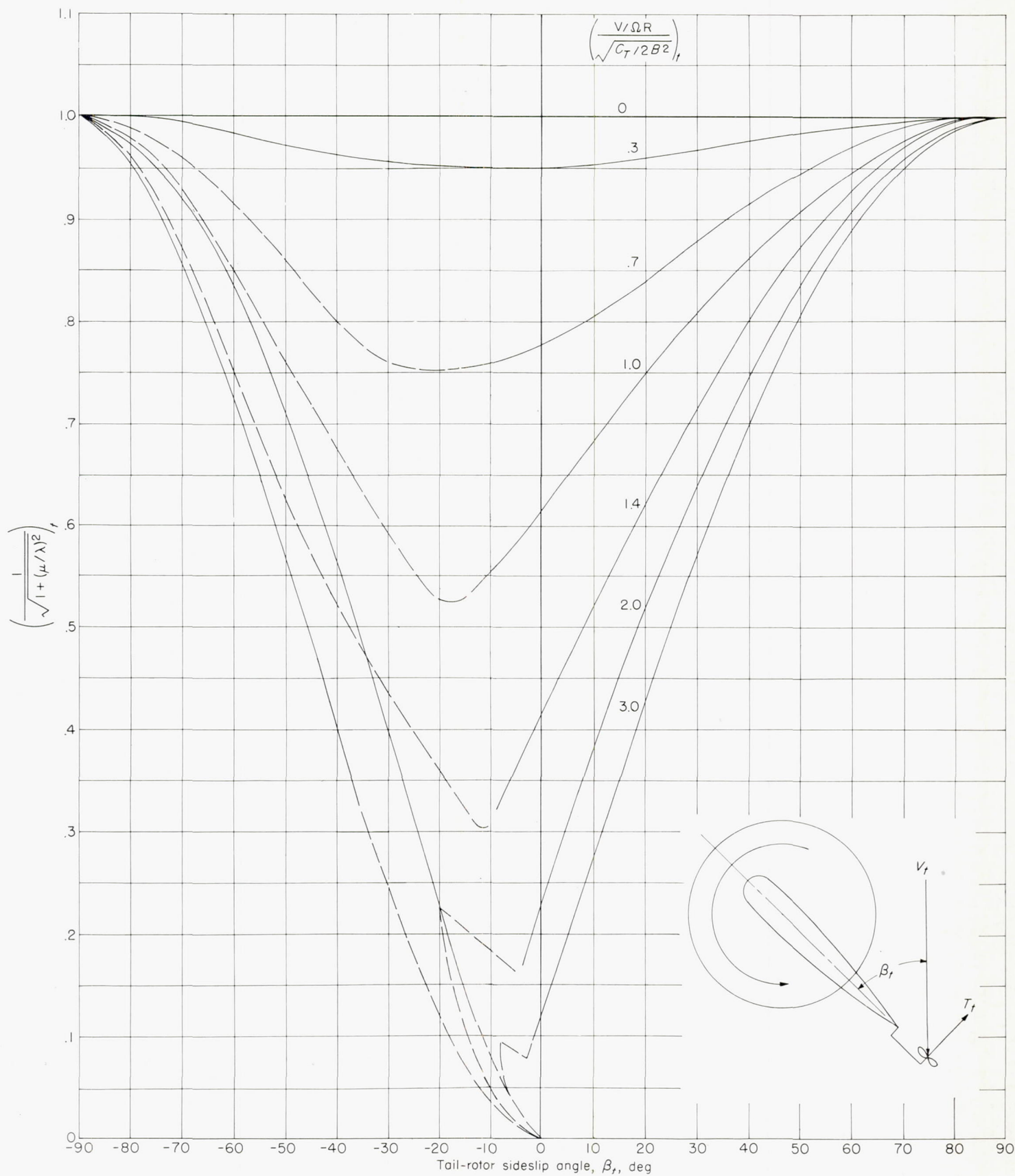


FIGURE 3.—Chart for determining  $\left( \frac{1}{\sqrt{1+(\mu/\lambda)^2}} \right)_t$ . Dashed lines indicate vortex region.

(A15) and (A16). For the vortex region, which is shown dashed, equation (A17) and figure 2 were used as discussed in appendix A. The limits of the vortex region in figure 3 are given by equations (A18) and (A19) which are plotted in figure 4.

#### RESPONSE TO PEDAL DEFLECTION

A complete tail-rotor study involves, in addition to charts of static rotor characteristics, an analysis that predicts the response of a helicopter to pedal deflection. Such an analysis, which derives the equation for the yaw of the helicopter following a step displacement of the pedals, is presented in appendix B. Associated main- and tail-rotor stability derivatives are also derived in appendix B. To simplify the analysis, two extreme cases are considered. In the first case, the rotor speed is assumed to remain constant during the yawing maneuver, whereas in the second case the rotor speed is assumed to vary enough that constant speed with respect to earth axes is maintained; that is,  $\Delta\Omega=r$ .

#### ILLUSTRATIVE CALCULATIONS

The use of the charts of figures 1 and 3 for tail-rotor design studies, as well as the pedal-response analysis, is illustrated by the sample calculations given below. The examples were chosen to be illustrative of the type required to investigate the ability of a helicopter to meet current flying-quality requirements. During the calculation of response to pedal deflection, the procedure for obtaining the rotor derivatives  $\frac{\partial C_{T/\sigma}}{\partial \theta}$  and  $\frac{\partial C_{T/\sigma}}{\partial \alpha}$  is illustrated.

The following characteristics are assumed:

Main rotor:	
$\Omega$ , radians/sec	20
$P_{hov}$ , hp	350
$P_{ihov} = 0.8P_{hov}$	
$v_{hov}$ , ft/sec	30
Direction of rotation (counterclockwise as viewed from above)	
$I_z$ , slug-ft <sup>2</sup>	2,000

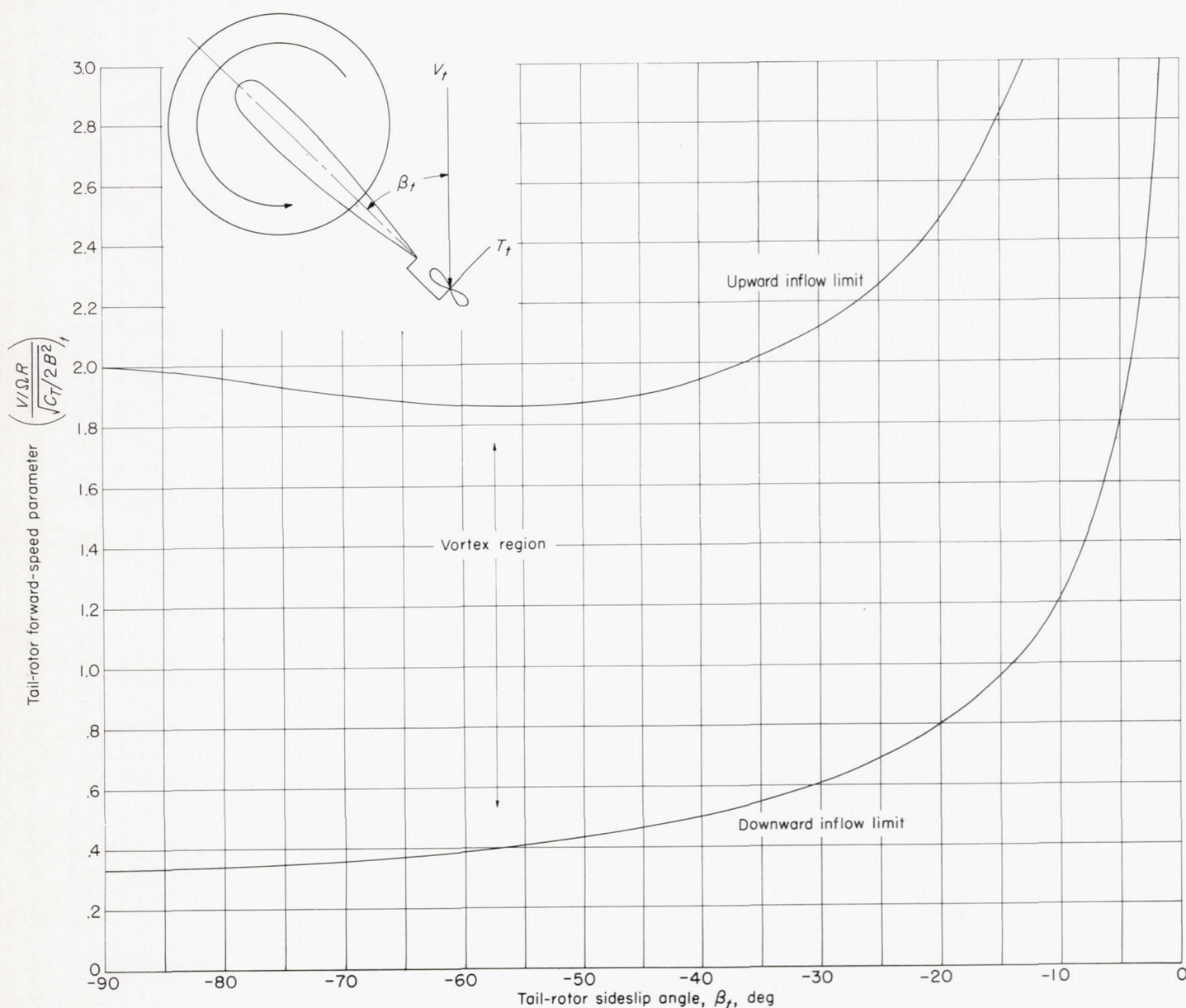


FIGURE 4.—Chart showing extent of vortex region in terms of tail-rotor forward-speed parameter  $\left(\frac{V/\Omega R}{\sqrt{C_T/2B^2}}\right)_t$  and tail-rotor sideslip angle  $\beta_t$ .

Tail rotor:

$\sigma$ .....	0.12
$\pi R^2$ , ft <sup>2</sup> .....	39.6
$l_t$ , ft.....	30
$\Omega R$ , ft/sec.....	565
Pitch range, deg.....	-5 to 15
$\theta_1$ , deg.....	-8
$[\sigma \rho \pi R^2 (\Omega R)^2 l_t]$ .....	108,000
Pedal travel, $\delta_r$ (right pedal reduces tail-rotor pitch), in.....	8

General:

$I_z$ (including mass of tail rotor), slug-ft <sup>2</sup> .....	5,000
Aerodynamic yawing moment (except where noted).....	0
$\rho$ .....	0.00238

## TAIL-ROTOR PITCH REQUIRED TO HOVER

Inasmuch as fuselage yawing moments are assumed equal to zero,

$$T_t = \frac{350 \times 550}{20 \times 30} = 321$$

$$C_{T_t} = \frac{321}{0.00238 \times 39.6 \times (565)^2} = 0.0107$$

$$(C_T/\sigma)_t = 0.089$$

Inasmuch as  $\mu=0$ ,

$$\left( \frac{1}{\sqrt{1+(\mu/\lambda)^2}} \right)_t = 1.0$$

Thus, from the chart of figure 1(d) for  $\left( \frac{\sigma}{\sqrt{1+(\mu/\lambda)^2}} \right)_t = 0.12$ , at  $\frac{V_t \sin \beta_t}{(\Omega R)_t} = 0$  and  $(C_T/\sigma)_t = 0.089$ ,  $\theta_{t_{\frac{3}{4}BR}} = 12.6^\circ$ .

## TAIL-ROTOR PITCH REQUIRED TO TURN OVER A SPOT IN A 30-KNOT (50.6 ft/sec) WIND

**Tail-rotor pitch required for trim at different sideslip angles.**—The first step in determining the tail-rotor pitch required to turn slowly over a spot in a 30-knot (50.6 ft/sec) wind is to find the tail-rotor thrust, which in turn depends on the main-rotor torque. The main-rotor torque may be found as follows:

$$\frac{V}{v_{hov}} = \frac{50.6}{30} = 1.69$$

By using this value of  $V/v_{hov}$ , figure 8 of reference 7 yields  $v/v_{hov} = P_t/P_{i_{hov}} = 0.64$ . Thus, the induced power required at 30 knots is  $P_t = 0.64 \times 0.8 \times 350 = 179$ . By assuming no change in the hovering value of profile-drag power, the total power required at 30 knots is then  $P = 0.2 \times 350 + 179 = 249$ .

By repeating the previous procedure,

$$T_t = \frac{249 \times 550}{20 \times 30} = 228 \text{ lb}$$

$$C_{T_t} = \frac{228}{0.094 \times (565)^2} = 0.0076$$

$$\left( \frac{C_T}{\sigma} \right)_t = \frac{0.0076}{0.12} = 0.0635$$

$$\left( \frac{C_T}{2B^2} \right)_t = 0.00404$$

$$\left( \frac{V}{\Omega R} \right)_t = 0.09$$

$$\left( \frac{V/\Omega R}{\sqrt{C_T/2B^2}} \right)_t = 1.4$$

From figure 3, values of  $\left( \frac{1}{\sqrt{1+(\mu/\lambda)^2}} \right)_t$  can be obtained for various values of  $\beta$ . (Inasmuch as  $r=0$ , then  $\beta=\beta_t$  and  $V=V_t$ .) Then, by interpolation between the charts of figure 1,  $\theta_{t_{\frac{3}{4}BR}}$  can be obtained. The computations are pre-

sented in table I. Similar computations were also made for 20-knot and 10-knot winds. The presentation of these results in graphical form is made in figure 5, in which is plotted the tail-rotor pitch required by the sample helicopter to hover at various sideslip angles in various winds. The vortex region for each curve is to the left of the flag.

TABLE I.—TAIL-ROTOR PITCH REQUIRED FOR TRIM AT DIFFERENT SIDESLIP ANGLES IN A 30-KNOT WIND

$$\left[ \left( \frac{V}{\Omega R} \right)_t = 0.09; \left( \frac{V/\Omega R}{\sqrt{C_T/2B^2}} \right)_t = 1.4; \left( \frac{C_T}{\sigma} \right)_t = 0.0635; \sigma_t = 0.12 \right]$$

$\beta_t$ , deg	$\frac{\sigma_t}{(\sqrt{1+(\mu/\lambda)^2})_t}$	$\left( \frac{V}{\Omega R} \right)_t \sin \beta_t$	$\theta_{t_{\frac{3}{4}BR}}$ , deg
0	0.050	0	7.8
10	.062	.016	9.0
20	.074	.031	10.2
30	.086	.045	11.4
40	.096	.058	12.4
50	.105	.069	13.3
60	.112	.078	14.0
70	.117	.085	14.7
80	.120	.089	15.1
90	.120	.090	15.1
-10	.037	-.016	6.9
-20	.043	-.031	7.2
-30	.052	-.045	7.5
-40	.062	-.058	8.0
-50	.075	-.069	8.1
-60	.090	-.078	8.4
-70	.104	-.085	8.4
-80	.116	-.089	9.0
-90	.120	-.090	9.4

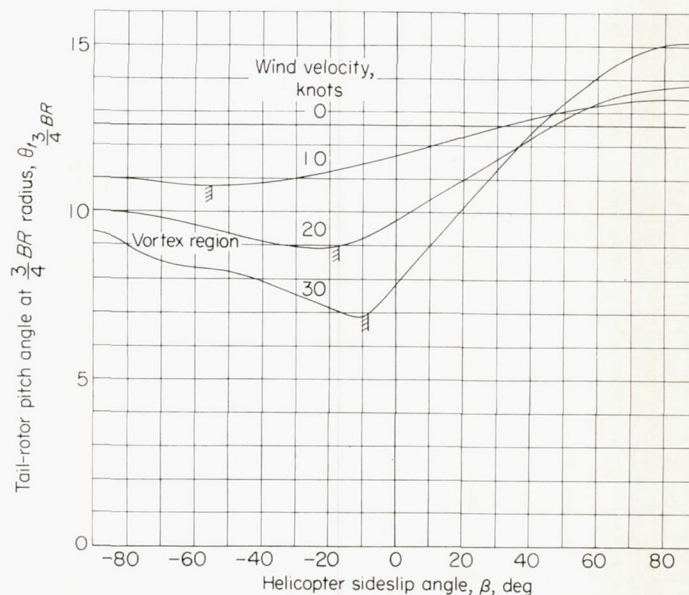


FIGURE 5.—Effect of forward speed and sideslip angle on tail-rotor pitch required for sample helicopter to hover over a spot. Vortex region for each curve is to the left of the flag.

**Tail-rotor pitch required to turn at a steady rate.**—In order to obtain information on the damping in yaw of the tail rotor, the tail-rotor pitch required to maintain a steady yawing velocity of 0.2 radian/sec, both to the left and to the right, during a turn in the 20-knot (33.7 ft/sec) wind will be computed subsequently. (The damping in yaw of the main rotor and fuselage will be neglected.)

For each sideslip angle  $\beta$ ,  $\beta_t$  and  $V_t$  are computed by using equations (B8) and (B9). Then, repeating the procedure for finding the tail-rotor thrust coefficient as was done for the 30-knot-wind case in the preceding section,

$$\left(\frac{C_T}{\sigma}\right)_t = 0.072$$

and

$$\left(\frac{V/\Omega R}{\sqrt{C_T/2B^2}}\right)_t = 0.88$$

The quantity  $\left(\frac{1}{\sqrt{1+(\mu/\lambda)^2}}\right)_t$  is then obtained from figure 3.

By using equation (B10),

$$\left(\frac{V \sin \beta}{\Omega R}\right)_t = \frac{V \sin \beta - l_t r}{(\Omega R)_t} = 0.06 \sin \beta - 0.01$$

Then, by interpolation between the charts of figure 1, the data in table II for  $V=20$  knots,  $r=0.2$  radian per second, were obtained. Similar computations, made for  $r=-0.2$  radian per second, are presented in graphical form (fig. 6) together with the results for the  $r=0$  case from figure 5.

#### RESPONSE TO PEDAL DEFLECTION WHILE HOVERING IN ZERO WIND

The yaw response per inch of rudder pedal deflection for the sample helicopter while hovering in zero wind will now be calculated. The stability derivatives needed for equations (B2) and (B3) will be determined from the charts of figures 1 and 3 for the two extreme assumptions that  $\Delta\Omega=0$  and  $\Delta\Omega=r$ . By assuming small displacements from trim, the derivatives will be computed at the trim condition,

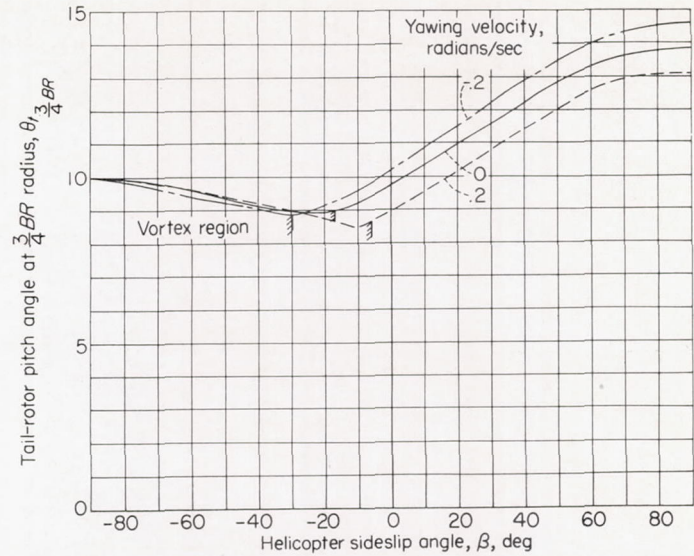


FIGURE 6.—Effect of helicopter rate of yaw on tail-rotor pitch required for trim at different sideslip angles ( $V=20$  knots). Vortex region for each curve is to the left of the flag.

which is

$$\left(\frac{\sigma}{\sqrt{1+(\mu/\lambda)^2}}\right)_t = 0.12, \quad (C_T/\sigma)_t = 0.89, \quad \left(\frac{V \sin \beta}{\Omega R}\right)_t = 0, \text{ and}$$

$$\theta_{t \frac{3}{4} BR} = 12.6^\circ.$$

The control derivative  $\partial N/\partial \theta_t$  is calculated by means of equation (B6) as follows:

$$\frac{\partial N}{\partial \theta_t} = \frac{\Delta N}{\Delta \theta_t} = -l_t \rho (\pi R^2)_t (\Omega R)_t^2 \sigma_t \left(\frac{\Delta C_T/\sigma}{\Delta \theta}\right)_t$$

For  $\left(\frac{\sigma}{\sqrt{1+(\mu/\lambda)^2}}\right)_t = 0.12$ , taking increments from the

$$(C_T/\sigma)_t = 0.06 \text{ line to the } (C_T/\sigma)_t = 0.10 \text{ line at } \frac{V_t \sin \beta_t}{(\Omega R)_t} = 0$$

$$\begin{aligned} \text{gives } \frac{\partial N}{\partial \theta_t} &= \frac{\Delta N}{\Delta \theta_t} = -30 \times 0.094 \times (565)^2 \times 0.12 \left(\frac{0.10 - 0.06}{13.6 - 9.6}\right) \\ &= -1,080 \frac{\text{lb-ft}}{\text{deg}} \end{aligned}$$

TABLE II.—TAIL-ROTOR PITCH REQUIRED TO TURN TO RIGHT OVER A SPOT IN A 20-KNOT WIND AT 0.2 RADIAN PER SECOND

$$\left[\left(\frac{V}{\Omega R}\right)_t = 0.06; \left(\frac{V/\Omega R}{\sqrt{C_T/2B^2}}\right)_t = 0.88; \left(\frac{C_T}{\sigma}\right)_t = 0.072; \sigma_t = 0.12; \frac{rl_t}{V} = 0.178\right]$$

$\beta$ , deg	$\frac{rl_t/V}{\cos \beta}$	$\tan \beta$	$\beta_t$ , deg	$V_t$	$\frac{V_t/\Omega R}{\sqrt{C_T/2B^2}}$	$\frac{\sigma_t}{\sqrt{1+(\mu/\lambda)^2}}$	$\left(\frac{V}{\Omega R}\right)_t \sin \beta$	$\left(\frac{V}{\Omega R}\right)_t \sin \beta_t$	$\theta_{t \frac{3}{4} BR}$ , deg
0	0.178	0	-10.1	34.3	0.89	0.077	0	-0.011	9.0
10	.181	.18	-3	32.2	.87	.081	.010	-.001	9.5
20	.190	.36	9.9	31.8	.83	.087	.020	.009	10.2
30	.205	.58	20.5	31.2	.82	.094	.030	.019	10.9
40	.233	.84	31.2	30.2	.78	.102	.038	.027	11.4
50	.277	1.19	42.3	29.3	.76	.108	.046	.035	11.9
60	.356	1.73	53.9	28.6	.74	.113	.052	.041	12.6
70	.520	2.75	65.9	28.2	.73	.116	.056	.045	13.0
80	1.025	5.67	77.9	27.8	.72	.119	.059	.048	13.1
90	-----	-----	90	27.8	.72	.120	.060	.049	13.1
-10	.181	-.18	-19.6	35.3	.92	.068	-.010	-.021	8.5
-20	.190	-.36	-29.0	36.3	.94	.076	-.020	-.031	8.8
-30	.205	-.58	-38.0	37.2	.97	.080	-.030	-.041	9.1
-40	.233	-.84	-47.1	37.9	.99	.088	-.038	-.049	9.3
-50	.277	-1.19	-55.7	38.5	1.00	.098	-.046	-.057	9.4
-60	.356	-1.73	-64.4	39.0	1.02	.107	-.052	-.063	9.6
-70	.520	-2.75	-73.0	39.2	1.02	.114	-.056	-.060	9.9
-80	1.025	-5.67	-81.5	39.7	1.03	.118	-.059	-.070	10.0
-90	-----	-----	-90	39.7	1.03	.120	-.060	-.071	10.0

The tail-rotor damping derivative is computed by means of equation (B11). The first part of the expression is obtained by taking increments from  $(C_T/\sigma)_t = 0.08$  to  $(C_T/\sigma)_t = 0.10$  along the  $\theta_{t_{BR}} = 12.6^\circ$  line in figure 1(d). The second part of the expression is zero for the present hovering-in-zero-wind case. Thus,

$$\begin{aligned} \left(\frac{\partial N}{\partial r}\right)_t &= \left(\frac{\Delta N}{\Delta r}\right)_t = -[\sigma l \rho (\Omega R)^2 \pi R^2]_t \left[ \frac{\partial (C_T/\sigma)_t}{\partial \left(\frac{V \sin \beta}{\Omega R}\right)_t} \left(-\frac{l}{\Omega R}\right)_t - \right. \\ &\quad \left. \left(\frac{l \cos \beta}{V}\right)_t \frac{\partial (C_T/\sigma)_t}{\partial \left(\frac{\sigma}{\sqrt{1+(\mu/\lambda)^2}}\right)_t} \sigma_t \frac{\partial \left(\frac{1}{\sqrt{1+(\mu/\lambda)^2}}\right)_t}{\partial \beta_t} \right] \\ &= -108,000 \left[ \frac{-30}{565} \frac{0.08-0.10}{0.022-(-0.023)} + 0 \right] \\ &= -2,550 \frac{\text{lb-ft}}{\text{radian/sec}} \end{aligned}$$

Inasmuch as  $V=0$ , then  $\frac{\partial N}{\partial \eta} = -\frac{\partial N}{\partial \beta} = 0$ .

For the assumption that  $\Delta\Omega=0$ , there is a damping contribution of the main rotor that is computed from equation (B12) as

$$\left(\frac{\partial N}{\partial r}\right)_m = -2 \frac{Q}{\Omega} = -\frac{2 \times 350 \times 550}{20 \times 20} = -960 \frac{\text{lb-ft}}{\text{radian/sec}}$$

By substituting into equation (B5) and taking  $I_z = 7,000$  slug-ft<sup>2</sup>, the value of  $c$  is found to be

$$c = \frac{-2550-960}{7000} = -0.50$$

Then, from equation (B4),

$$\frac{\eta}{\Delta\theta_t} = -35(e^{-0.50t} + 0.50t - 1)$$

For  $t=1$  second,

$$\frac{\eta(t=1)}{\Delta\theta_t} = -3.7 \text{ deg/deg}$$

Thus, for the assumption that  $\Delta\Omega=0$ , the displacement in yaw per inch of pedal travel at  $t=1$  second is

$$\frac{\eta(t=1)}{\Delta\delta_r} = -3.7 \frac{\text{deg}}{\text{deg}} \times \frac{20 \text{ deg}}{-8 \text{ in.}} = 9.3 \frac{\text{deg}}{\text{in.}}$$

where the  $-8$  inches is the total rudder pedal deflection corresponding to the total pitch range of  $20^\circ$ .

For the assumption that  $\Delta\Omega=r$ ,  $I_z$  is now equal to  $5,000$  slug-ft<sup>2</sup>,  $\Delta N/\Delta\theta_t$  is unchanged, and  $(\partial N/\partial r)_m = 0$ . Inasmuch as, at trim,  $(V \sin \beta)_t = 0$ , the additional damping in yaw of the tail rotor because of its variation in speed is (as pointed out in appendix B) equal to  $(\partial N/\partial r)_m$  computed under the assumption that  $\Delta\Omega=0$ . Thus,

$$\Delta\left(\frac{\partial N}{\partial r}\right)_t = -960 \frac{\text{lb-ft}}{\text{radian/sec}}$$

Then, by substituting into equation (B5),

$$c = \frac{-2550-960}{5000} = -0.70$$

and, from equation (B4),

$$\frac{\eta}{\Delta\theta_t} = -25(e^{-0.70t} + 0.70t - 1)$$

For  $t=1$  second,

$$\frac{\eta(t=1)}{\Delta\theta_t} = -4.9 \text{ deg/deg}$$

or

$$\frac{\eta(t=1)}{\Delta\delta_r} = -4.9 \times \frac{20}{-8} = 12.3 \text{ deg/in.}$$

For  $(V \sin \beta)_t = 0$ , the only difference in the exponential equation for  $\eta/\Delta\theta_t$  resulting from the use of the two different rotor-speed assumptions arises from the use of a smaller moment-of-inertia value in the  $\Delta\Omega = r$  case. If the moment of inertia of the main rotor is relatively large compared with that of the fuselage, the more conservative assumption should be used for design purposes. In the present illustrative example, inasmuch as the values of yaw displacement computed for the two different rotor-speed assumptions do not differ very much, the average value is used. Thus, for the sample helicopter in hovering at zero wind, the displacement in yaw per inch of pedal travel at  $t = 1$  second is

$$\frac{\eta(t=1)}{\Delta\delta_r} = \frac{9.3+12.3}{2} = 10.8 \text{ deg/in. pedal}$$

In figure 7 are shown, for the sample helicopter, time histories of response to a 1-inch step displacement of the rudder pedals while hovering in zero wind. The curves were obtained from the computed equations for  $\eta/\Delta\theta_t$  which were derived on the alternate assumptions of constant rotor speed and  $\Delta\Omega = r$ . At  $t = 1$  second, the average value of  $\eta$  is  $10.8^\circ$ , as determined previously.

#### RESPONSE TO PEDAL DEFLECTION WHILE HOVERING IN 30-KNOT WIND

There will now be computed the tail-rotor pitch required to satisfy the requirement of reference 1 that the helicopter, while trimmed at the most critical yaw angle during hovering in a 30-knot wind, achieve  $3^\circ$  of yaw in the first second following full pedal deflection in the critical direction.

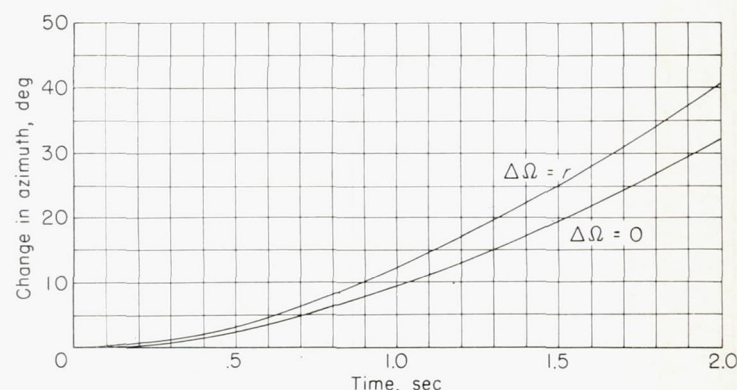


FIGURE 7.—Response of sample helicopter in hovering to a 1-inch step displacement of pedals.

For the sample helicopter, table I indicates that the critical yaw angle during hovering in a 30-knot wind is  $90^\circ$  left yaw (right sideslip) at which time  $15.1^\circ$  of tail-rotor pitch is required. In order to illustrate a less simplified case, it will be assumed, however, that because of fuselage yawing moments the critical angle is  $60^\circ$  right sideslip and there is an aerodynamic yawing moment to the right of 1,500 pound-feet acting on the fuselage. Thus, before proceeding with the response-to-pedal-deflection calculations, it is first necessary to calculate the pitch angle required to trim at the new critical yaw angle of  $60^\circ$ .

**Determination of new trim value of tail-rotor pitch.**—By repeating the procedure used in a previous section for computing the pitch required for trim while hovering in a 30-knot wind, but taking the fuselage yawing moment into account, the following equations are given:

$$\beta_t = 60^\circ$$

$$T_t = 228 + \frac{1500}{30} = 278 \text{ lb}$$

$$C_{T_t} = 0.0093$$

$$(C_{T/\sigma})_t = 0.0775$$

$$(C_{T/2B^2})_t = 0.00494$$

$$(V/\Omega R)_t = 0.090$$

$$\left(\frac{V/\Omega R}{\sqrt{C_{T/2B^2}}}\right)_t = 1.28$$

From figure 3,

$$\left(\frac{1}{\sqrt{1+(\mu/\lambda)^2}}\right)_t = 0.935$$

Thus,

$$\left(\frac{\sigma}{\sqrt{1+(\mu/\lambda)^2}}\right)_t = 0.112$$

Interpolating between the charts of figure 1 for  $\left(\frac{\sigma}{\sqrt{1+(\mu/\lambda)^2}}\right)_t$ ,  $= 0.09$  and  $0.12$ , for  $\left(\frac{V \sin \beta}{\Omega R}\right)_t = 0.0785$  and  $(C_{T/\sigma})_t = 0.0775$ , gives  $\theta_{t_{\frac{3}{4}BR}} = 15.5^\circ$ . Thus, the new trim value of tail-rotor pitch is  $15.5^\circ$  instead of  $15.1^\circ$ , which was calculated for the case of zero assumed fuselage yawing moment.

**Computation of tail-rotor pitch required to maneuver.**—The calculation of the additional amount of tail-rotor pitch required to achieve  $3^\circ$  of yaw in the first second following full pedal deflection will be carried out, as in the previously described calculations of a step-pedal maneuver in zero wind, under the alternate assumptions of constant rotor speed and a variation of rotor speed equal to the yawing velocity.

By assuming constant rotor speed, the stability derivatives needed for equations (B2) and (B3) are determined in a manner similar to that carried out for the zero-wind case as follows:

From equation (B6),

$$\frac{\partial N}{\partial \theta_t} = -1,090 \frac{\text{lb-ft}}{\text{deg}}$$

From equation (B12),

$$\left(\frac{\partial N}{\partial r}\right)_m = -690 \frac{\text{lb-ft}}{\text{radian/sec}}$$

From equation (B11),

$$\begin{aligned} \left(\frac{\partial N}{\partial r}\right)_t = & -108,000 \left[ \frac{-30}{565} \frac{-0.02}{0.031} + \right. \\ & \left. \frac{-0.008}{0.03} 0.12 \frac{0.004}{1/57.3} \left( -\frac{30 \times 0.5}{50.6} \right) \right] = -3,900 \frac{\text{lb-ft}}{\text{radian/sec}} \end{aligned}$$

Although the aerodynamic fuselage moment is assumed to remain unchanged during the pedal-deflection maneuver, there is a change in the static-directional stability of the tail rotor. This derivative is found by substituting into equation (B14) values for known constants and slopes obtained by interpolation between the 0.09 and 0.12 charts of figure 1 and from figure 3. Thus,

$$\begin{aligned} \frac{\partial N}{\partial \beta} = & -\frac{-0.040}{0.060} 108,000 \times 0.090 \cos 60^\circ - \\ & \frac{-0.006}{0.03} 0.12 \times 108,000 \times 0.004 \times 57.3 \\ = & 3,240 + 590 = 3,830 \text{ lb-ft/radian} \end{aligned}$$

For turns over a spot,

$$\frac{\partial N}{\partial \eta} = -\frac{\partial N}{\partial \beta} = -3,830 \text{ lb-ft/radian}$$

Substituting the calculated derivatives into equation (B3) gives

$$s^2 - \frac{-3900 - 690}{5000 + 2000} s - \frac{-3830}{5000 + 2000} = 0$$

By solving for the complex roots  $a \pm bi$ ,

$$a = -0.33$$

and

$$b = 0.66$$

Substituting into equation (B2) gives

$$\frac{\eta}{\Delta \theta_t} = -16.3 [e^{-0.33t} (-0.50 \sin 0.66t - \cos 0.66t) + 1]$$

For  $t = 1$  second,

$$\frac{\eta(t=1)}{\Delta \theta} = -3.4 \text{ deg/deg}$$

Thus, under the assumption of constant rotor speed,  $\frac{3 \text{ deg}}{3.4 \text{ deg/deg}} = 0.88^\circ$  of additional tail-rotor pitch would be required to achieve  $3^\circ$  of yaw in the first second following the pedal displacement.

Under the assumption that  $\Delta\Omega=r$ , the calculation would proceed as follows:

$$I_z=5,000$$

$$\frac{\Delta N}{\Delta\theta_i} \text{ is unchanged}$$

$$\left(\frac{\partial N}{\partial r}\right)_m=0$$

$$\left(\frac{\partial N}{\partial \eta}\right) \text{ is unchanged}$$

The additional damping in yaw due to variations in tail-rotor speed is obtained from equation (B20). The derivative

$$\frac{\partial(C_T/\sigma)_t}{\partial\left(\frac{V \sin \beta}{\Omega R}\right)_t} \text{ has already been obtained for } \partial N/\partial \beta. \text{ Thus,}$$

$$\Delta\left(\frac{\partial N}{\partial r}\right)_t = -30\left(\frac{0.040}{0.060} 0.0785 \frac{3600}{20} + \frac{2 \times 278}{20}\right) = -1,110$$

Substituting into equation (B3) gives

$$s^2 - \frac{-3900-1110}{5000} s - \frac{-3830}{5000} = 0$$

$$a = -0.50$$

and

$$b = 0.72$$

Thus, by substituting into equation (B2),

$$\frac{\eta}{\Delta\theta_i} = 16.3 [e^{-0.50} (-0.70 \sin 0.72t - \cos 0.72t) + 1]$$

For  $t=1$  second,

$$\frac{\eta(t=1)}{\Delta\theta_i} = -4.2 \text{ deg/deg}$$

The additional pitch required would then be

$$\frac{3 \text{ deg}}{4.2 \text{ deg/deg}} = 0.71^\circ.$$

**Tail-rotor pitch needed to satisfy requirement of reference 1.**—Taking an average of the answers for the two different assumptions gives

$$\Delta\theta_i = \frac{0.88+0.71}{2} = 0.8^\circ$$

Thus, in order to achieve the required  $3^\circ$  of yaw in the first second,  $0.8^\circ$  of additional tail-rotor pitch would be required. The total value of  $\theta_i$  needed to satisfy the requirement of reference 1 is, therefore,

$$\theta_i = 15.5^\circ + 0.8^\circ = 16.3^\circ$$

#### DISCUSSION OF ILLUSTRATIVE CALCULATIONS

Some significant characteristics of low-speed tail-rotor directional stability and control can be deduced from the sample calculations made herein.

#### DIRECTIONAL STABILITY AND DAMPING IN YAW

The curves of figure 5 indicate that, if fuselage directional stability characteristics are neglected and tail-rotor thrust is assumed to act toward the right, the typical single-rotor helicopter at speeds below 10 knots is directionally stable from approximately  $50^\circ$  left sideslip to about  $90^\circ$  right sideslip. For speeds higher than about 10 knots, the stability characteristics during sideslip in the direction of tail-rotor thrust are similar, the directional stability increasing with speed. For sideslip in the direction opposite to tail-rotor thrust, however, a directional instability appears, as a result of the tail rotor entering the vortex region. The curves in figure 6 indicate that, although the damping in yaw at 20 knots is normally stable, in the vortex region the damping in yaw is approximately zero, or even slightly unstable. Similar curves for 30 knots indicate large erratic variations in damping in yaw, from unstable to stable, in the vortex region. Also, although it is not shown by the curves of figures 5 and 6, reference 8 gives evidence that the vortex region corresponds to an unsteady-flow condition.

Inasmuch as the axial component of velocity through the tail rotor depends upon the sine of the sideslip angle, the curves of figures 5 and 6 can be used for the entire azimuth range of  $\pm 180^\circ$ . For example, at  $\beta=160^\circ$ , the tail-rotor pitch is the same as at  $\beta=20^\circ$ .

#### RESPONSE TO STEP PEDAL DEFLECTION

The time history of figure 7 is typical of first-order single-degree-of-freedom systems inasmuch as  $\frac{\partial N}{\partial \eta}=0$ . Initially, the rate of displacement depends primarily on the inertia, whereas later it depends primarily on the damping. At all times, the displacement depends upon the control moment. Thus, by calling for a specific yaw-angle range in 1 second, requirements such as those of reference 1 insure against insufficient or excessive control moment in relation to the inertia and damping in yaw. Preliminary study of yaw control in near-hovering flight indicates that the pilot probably expects the yaw displacement to be within certain limits a short time after a reasonable pedal motion.

For the sample helicopter in hovering, the yaw response at the end of the first second was calculated to be  $10.8^\circ$  yaw per inch of pedal displacement. Preliminary flying-quality studies indicate that, if the pedals have large friction and out-of-trim forces, such a response may be too high. Of course, reduction in pedal friction and incorporation of a trimming device would help. If, however, the yaw control were still too sensitive, a possible solution might be the incorporation of a mixing linkage in the tail-rotor control such that collective pitch or throttle motion would also produce a tail-rotor pitch change. Then the pitch change per inch of pedal could be reduced. Another advantage of such a mixing linkage is that it would reduce the coordination necessary between pitch lever and pedals during hovering at different wind speeds. Reducing the sensitivity of the sample helicopter by increasing pedal travel is not feasible, inasmuch as the travel is already a typical value of 8 inches.

From the calculation of response to pedal deflection in a 30-knot wind, it was found that  $16.3^\circ$  of tail-rotor pitch

would be required for the sample helicopter to meet one of the requirements of reference 1. This requirement calls for the ability, while trimmed at the most critical yaw position in a 30-knot wind, to achieve at least  $3^\circ$  of yaw in the first second following full displacement of the pedals in the critical direction. By use of figures 1 and 3, the minimum pitch at which the tail rotor would start to stall in the range from 0 to 30 knots was found to be about  $18\frac{1}{2}^\circ$ . Thus, it appears that the tail rotor of the sample helicopter could be rigged to give the required pitch without danger of stalling.

#### COMPARISON OF THEORY WITH EXPERIMENTAL RESULTS

In order to study the adequacy of the charts presented herein, a comparison of the theory was made with experimental results. In figure 8 are presented plots of pedal position against sideslip angle during fairly rapid turns over a spot in a wind of approximately 13 knots for the single-rotor helicopter shown in figure 9. This helicopter has characteristics that are generally similar to the sample helicopter characteristics used herein. The sideslip angle was obtained by integrating measured yawing-velocity records. In figure 8 are also presented theoretical curves of pedal position against sideslip angle computed from the charts herein for the helicopter of figure 9 for the first half of the turn in each direction. (Only the first half of the turn is computed because the experimental sideslip angles during the second half of the turn are inaccurate because of the accumulation of integration errors.) The assumption that  $\Delta\Omega=r$  was used in calculating the theoretical curves, but, for simplicity, the additional damping in yaw of the tail rotor due to changes in rotational speed was neglected, as were fuselage yawing moments. The tail-rotor thrust was corrected for measured yawing acceleration.

During the turn to the left, the measured pedal position varies rather smoothly throughout the entire maneuver. However, during the early part of the turn to the right large and rapid pedal displacements are indicated. The resultant velocity and sideslip angle at the tail rotor, corrected for yawing velocity, were computed during the computation of the theoretical curves. Comparison with figure 4 indicated that, during the turn to the left, the tail rotor never entered the vortex region; whereas during the turn to the right, it did. The range of sideslip angle for which the tail rotor was within the vortex region based on figure 4 is indicated in figure 8(b). It can be seen that the large and rapid pedal motions all occurred while the tail rotor was in the vortex region. The pilot's effort when the tail rotor is operating in the vortex region is increased, probably because, as indicated previously, the flow conditions there are unsteady and the damping in yaw is low or unstable.

The qualitative correlation of the theoretically and experimentally indicated extent of the vortex region gives some confidence in the accuracy of the downward inflow limit of the vortex region in the theoretical curves herein. As indicated in appendix A, this limit was based on the indication of reference 8 that the vortex region begins when the axial component of velocity is approximately 40 percent of the inflow velocity.

This region of difficult tail-rotor control that results when the tail rotor enters the vortex region is similar to that which is experienced when the main rotor enters the vortex region during partial-power descent at zero or low forward speeds. Knowledge of the existence of this region of difficult tail-rotor control should be of value to pilots, in that they would not expect to achieve steady conditions in this region and hence would try to avoid prolonged operation therein when feasible.

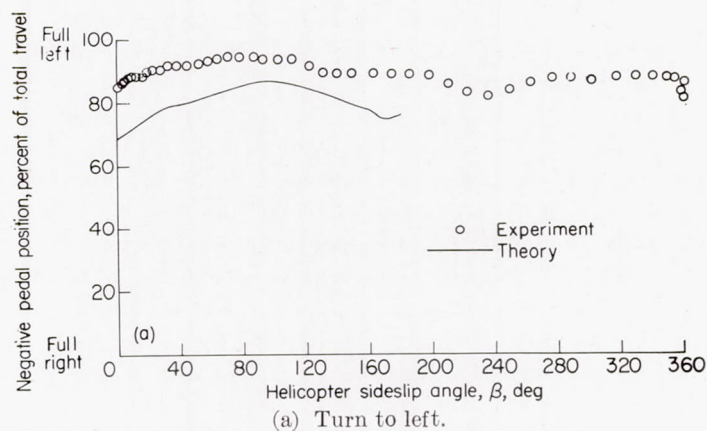


FIGURE 8.—Measured pedal position against sideslip angle during fairly rapid turns over a spot in a wind of 13 knots for helicopter of figure 9 and comparison with theory. Data points are  $\frac{1}{2}$  second apart.

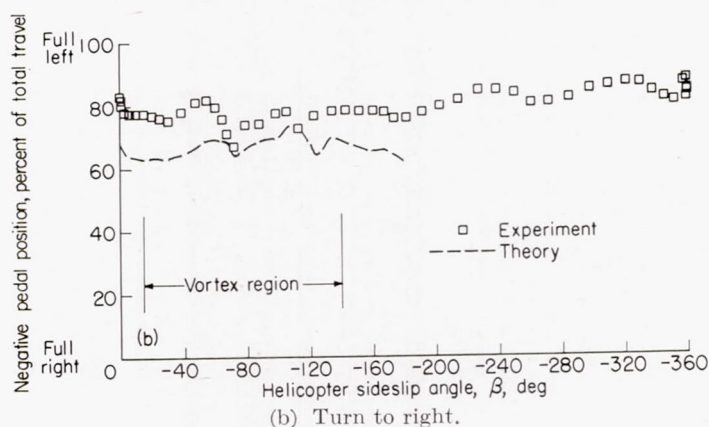


FIGURE 8.—Concluded.

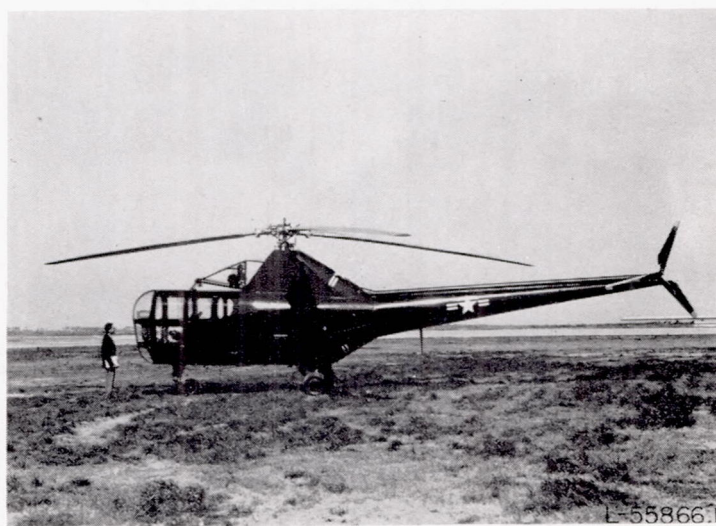


FIGURE 9.—Helicopter on which data of figure 8 were obtained.

For a particular helicopter, the regions of forward speed and sideslip angle in which tail-rotor control difficulty may be experienced can be computed from figure 4. Limited unpublished flight data indicate the vortex region to be less potent, or perhaps even nonexistent, at the higher forward speeds covered in figure 4. The large component of velocity perpendicular to the rotor shaft at the higher forward speeds may reduce or eliminate the formation of this type of flow. However, until a more thorough experimental investigation establishes an upper speed limit to the vortex region, the entire vortex region of figure 4 may well be considered as a region of potential difficulty.

At  $0^\circ$  angle of sideslip, the theoretical curves of figure 8 indicate about 15 percent more right pedal, or about  $3^\circ$  less pitch, than the experimental curves. Some of this difference is thought to be due to the experimental pitch being lower than that indicated by pedal position because of play and distortion in the tail-rotor control system. At high values of tail-rotor pitch, a large left pedal force is required along with the left pedal deflection, indicating a large pitch-reducing tendency in the tail rotor. Also, the effectiveness of the root portion of the tail-rotor blade is probably reduced somewhat by the exposed heads of the bolts used to attach the blade to the root fitting. In addition, calculations indicate the taper of the tail-rotor blades, which was neglected in the theoretical derivatives herein, causes the theory to underestimate somewhat the tail-rotor collective pitch. All these conditions cause the theory to underestimate the required tail-rotor pitch. Thus, for design purposes, these factors must be accounted for, either rationally or empirically.

For the turn to the left, the shape of the theoretical curve compares well with that of the experimental curve, except for somewhat higher slopes. The difference in slope indicates that the fuselage is unstable directionally.

For the turn to the right, the theoretical curve does not match the experimental curve as well. This situation is to be expected because of the unsteady flow conditions in the vortex region.

This comparison between measured and theoretical tail-rotor pitch during fairly rapid turns over a spot indicates the charts and procedures herein to be useful for computing either the change in tail-rotor pitch needed for a given dynamic maneuver or the motion of the helicopter due to pedal deflection.

#### CONCLUDING REMARKS

Theoretically derived charts and equations have been presented by which tail-rotor design studies of directional trim and control response at low forward speeds (i.e., at tip-speed ratios less than 0.10) can be conveniently made. These charts can also be used to determine the main-rotor stability derivatives of the ratio of thrust coefficient to solidity with respect to pitch angle and rotor angle of attack at low forward speeds.

Studies made with the charts and confirmed by flight tests indicate a region of difficulty of tail-rotor control at various combinations of forward speed and sideslip angle similar to that which has been experienced on main rotors during partial-power descent at zero or low forward speed. It appears desirable to avoid prolonged operation in this region.

The measured variations of tail-rotor pitch during a moderately rapid turn over a spot in a wind can be fairly well predicted theoretically.

LANGLEY AERONAUTICAL LABORATORY,  
NATIONAL ADVISORY COMMITTEE FOR AERONAUTICS.  
LANGLEY FIELD, VA., *October 27, 1953.*

## APPENDIX A

### THEORETICAL DEVELOPMENT—STATIC ROTOR CHARACTERISTICS

In this appendix, equations for the collective pitch of a tail rotor at low forward speeds are derived in terms of its forward speed, tip speed, sideslip angle, thrust coefficient, solidity, and the yawing velocity of the helicopter. These equations are used to derive charts from which the tail-rotor directional-stability, directional-control, and damping-in-yaw derivatives can be obtained.

#### ASSUMPTIONS

**Uniform inflow.**—The inflow through the rotor is assumed to be uniform. The effect of a radial variation in inflow is discussed later. Reference 3 indicates no appreciable effect of longitudinal inflow asymmetry on thrust at fixed values of pitch and average inflow.

**Isolation of tail rotor.**—At some forward speed the tail rotor enters the downwash field of the main rotor. The effects of operating in the main-rotor downwash field are neglected, inasmuch as the primary effect is a change in the direction of flight of the tail rotor. The effect of tail-rotor supporting structures and the proximity of tail surfaces is also neglected.

**Neglect of  $\mu^2$  with respect to unity.**—The assumption is now made that  $\mu$  is less than 0.10 and, therefore,  $\mu^2$  is much less than 0.01. Thus, neglect of  $\mu^2$  with respect to unity causes a maximum error in each term of about 1 percent. The term  $(\mu/\lambda)^2$ , however, is not negligible with respect to unity.

**Assumptions of references 3 and 4.**—Inasmuch as the derivatives in this report are based on the equations of references 3 and 4, the assumptions of these references are automatically incorporated herein.

#### DEVELOPMENT OF EQUATIONS

Inasmuch as  $\theta_{3/4BR} = \theta_0 + 0.75B\theta_1$ , and  $\mu^2$  is assumed to be much less than 1 ( $\mu^2 \ll 1$ ), equation (6) of reference 4 can be rewritten as follows:

$$\frac{2C_T}{\sigma a} = \frac{B^2}{2} \lambda + \frac{B^3}{3} \theta_{3/4BR} \quad (A1)$$

Equation (7) of reference 4 can be rewritten as follows:

$$\frac{V}{\Omega R} \sin \alpha = \lambda + \frac{C_T}{2|\lambda|B^2\sqrt{1+(\mu/\lambda)^2}} \quad (A2)$$

Since the last term represents rotor induced velocity, absolute bars have been added to  $\lambda$  in order to make the expression always positive. Also,  $B^2$  has been added in the denominator of the last term in order to provide consistency with forward flight analyses, wherein it is assumed that the rotor is effective only in producing thrust out to  $BR$ .

For the normal working state of a rotor wherein  $\lambda$  is negative, equation (A2) can be solved for  $\lambda$  as follows:

$$\lambda = \frac{V}{\Omega R} \frac{\sin \alpha}{2} - \frac{1}{2} \sqrt{\left(\frac{V}{\Omega R} \sin \alpha\right)^2 + \frac{2}{B^2} \frac{C_T}{\sigma} \frac{\sigma}{\sqrt{1+(\mu/\lambda)^2}}} \quad (A3)$$

Substitution of equation (A3) into equation (A1) and solving for  $\theta_{3/4BR}$  gives, for negative  $\lambda$ ,

$$\theta_{3/4BR} = \frac{3}{2B} \left[ \frac{1}{2} \sqrt{\left(\frac{V}{\Omega R} \sin \alpha\right)^2 + \frac{2}{B^2} \frac{C_T}{\sigma} \frac{\sigma}{\sqrt{1+(\mu/\lambda)^2}}} + \frac{4}{aB^2} \frac{C_T}{\sigma} - \frac{V \sin \alpha}{\Omega R} \right] \quad (A4)$$

In order to put equation (A4) into a more convenient form for tail rotors,  $\theta_{3/4BR}$  will be expressed in degrees, and instead of the angle of attack  $\alpha$ , the sideslip angle  $\beta$  will be used. For the case of counterclockwise main-rotor rotation, the tail-rotor thrust is to the right for the conventionally powered helicopter. Thus,  $\alpha$  for the tail rotor is equal to  $-\beta$ , where  $\beta$  is positive for sideslip to the right. (In the jet-powered helicopter, the tail-rotor thrust required to overcome the friction torque will act to the left for counterclockwise main-rotor rotation, in which case  $\alpha = \beta$ . The sign convention corresponding to the conventionally powered helicopter will be followed in this report.) Also, a yawing velocity of the helicopter will cause an additional flow through the tail rotor. Thus, the expression  $\frac{V}{\Omega R} \sin \alpha$  becomes  $-V_t \sin \beta_t / (\Omega R)_t$ , where  $V_t$  and  $\beta_t$  are, respectively, the velocity and sideslip angle at the tail rotor including the effect of yawing velocity. Thus, equation (A4) becomes, for negative  $\lambda$ ,

$$\theta_{3/4BR} = 57.3 \frac{3}{2B} \left[ \frac{1}{2} \sqrt{\left(\frac{V \sin \beta}{\Omega R}\right)_t^2 + \frac{2}{B^2} \frac{C_T}{\sigma} \frac{\sigma}{\sqrt{1+(\mu/\lambda)^2}}} + \frac{4}{aB^2} \frac{C_T}{\sigma} + \frac{1}{2} \left(\frac{V \sin \beta}{\Omega R}\right)_t \right] \quad (A5)$$

For those conditions where  $\lambda$  is positive, repeating the steps for equations (A3) to (A5) gives

$$\theta_{3/4BR} = 57.3 \frac{3}{2B} \left[ -\frac{1}{2} \sqrt{\left(\frac{V \sin \beta}{\Omega R}\right)_t^2 + \frac{2}{B^2} \frac{C_T}{\sigma} \frac{\sigma}{\sqrt{1+(\mu/\lambda)^2}}} + \frac{4}{aB^2} \frac{C_T}{\sigma} + \frac{1}{2} \left(\frac{V \sin \beta}{\Omega R}\right)_t \right] \quad (A6)$$

## VALIDITY OF UNIFORM INFLOW ASSUMPTION

Comparison of equation (A4) with equation (A17) of reference 5 indicates that  $\theta_{\frac{3}{4}BR}$  for a linearly twisted rotor blade in vertical climb where  $\mu=0$  and  $\sin \alpha=-1$  is equal to  $\theta_{\frac{2}{3}BR}$  for an ideally twisted rotor in vertical climb (at equal values of  $C_T$ ,  $\sigma$ , and  $V/\Omega R$ ). From a study of figure 1 of reference 6, it can be seen that, at least for the special case of hovering, a solution for  $\theta_{\frac{3}{4}BR}$  for a linearly twisted rotor including radial inflow variations shows that the pitch angle at  $\frac{3}{4}BR$  is very close to  $\theta_{\frac{2}{3}BR}$  for the ideally twisted rotor. (In fig. 1 of ref. 6,  $B=1.0$ .) Thus, the assumption made herein of uniform inflow is indicated to give reasonably correct answers for  $\theta_{\frac{3}{4}BR}$ .

## BLADE-STALL LIMITS

The theory becomes inaccurate when blade sections start to stall. In order to give some idea of the section angles of attack, the section angle of attack in the hovering or vertical-flight condition at  $\frac{2}{3}BR$  is computed. This radius was chosen because it is reasonably representative, and because it is easily computed. The computation is as follows: From equation (27) of reference 4,

$$\alpha_{\frac{2}{3}BR} = \theta_{\frac{2}{3}BR} + \frac{\lambda}{\frac{2}{3}B} = \theta_{\frac{3}{4}BR} + \left(\frac{2}{3}B - \frac{3}{4}B\right)\theta_1 + \frac{\lambda}{\frac{2}{3}B} \quad (A7)$$

Substituting for  $\lambda$  from equation (A1) gives

$$\alpha_{\frac{2}{3}BR} = \frac{6}{aB^3} \frac{C_T}{\sigma} - \left(\frac{3}{4}B - \frac{2}{3}B\right)\theta_1 \quad (A8)$$

For  $\alpha$  and  $\theta_1$  in degrees, setting  $a=5.73$  and  $B=0.97$ ,

$$\alpha_{\frac{2}{3}BR} = 65.7 \frac{C_T}{\sigma} - 0.08\theta_1 \quad (A9)$$

## VORTEX REGION

In reference 8 it was reported that, for the test helicopter of the reference, unsteady conditions were experienced at vertical rates of descent above about 500 ft/min. The inflow velocity (i.e., resultant velocity through rotor disk) at this rate of descent is computed to be approximately 1,200 ft/min. Thus, it is assumed that the momentum theory used in the rotor theory of references 3 and 4 is good until the axial component of free-stream velocity upward with respect to the rotor equals 500/1200, which is approximately equal to 40 percent of the inflow velocity.

Reference 9, page 127, indicates that, when the upward free-stream velocity exceeds a certain value, the air flow near the blade tips takes on the shape of a vortex ring instead of existing in the form of a simple slipstream; thus the unsteady flow conditions mentioned previously are taken into account. This unsteady flow region, in which the momentum theory is inapplicable, is referred to as the vortex region. In reference 9, page 131, the momentum theory used in the

rotor theory of references 3 and 4 is indicated to become good again when the axial component of flight velocity upward through the rotor is equal to twice the inflow velocity.

Inasmuch as the momentum theory used in references 3 and 4 (and, hence, in this report) is not valid in the vortex region, an empirical procedure is used to obtain solutions of tail-rotor collective pitch in this region. This procedure is based on the use of empirical curves relating vertical flight speed to induced velocity in the vortex region and is outlined as follows: Dividing the three terms in equation (A2) by

$$\sqrt{\frac{C_T}{2B^2\sqrt{1+(\mu/\lambda)^2}}}$$

and using the angle  $\beta_i$  instead of the angle  $\alpha$  gives, for negative  $\lambda$ ,

$$\left(\frac{V \sin \beta/\Omega R}{\sqrt{\frac{C_T}{2B^2\sqrt{1+(\mu/\lambda)^2}}}}\right)_t = -\left(\frac{\lambda}{\sqrt{\frac{C_T}{2B^2\sqrt{1+(\mu/\lambda)^2}}}}\right)_t + \left(\frac{\sqrt{\frac{C_T}{2B^2\sqrt{1+(\mu/\lambda)^2}}}}{\lambda}\right)_t \quad (A10)$$

and, for positive  $\lambda$ ,

$$\left(\frac{V \sin \beta/\Omega R}{\sqrt{\frac{C_T}{2B^2\sqrt{1+(\mu/\lambda)^2}}}}\right)_t = -\left(\frac{\lambda}{\sqrt{\frac{C_T}{2B^2\sqrt{1+(\mu/\lambda)^2}}}}\right)_t - \left(\frac{\sqrt{\frac{C_T}{2B^2\sqrt{1+(\mu/\lambda)^2}}}}{\lambda}\right)_t \quad (A11)$$

For vertical climb or descent ( $\mu=0$ ;  $\sin \beta_i=\pm 1$ ), equations (A10) and (A11) correspond to the computed portions of figure 8 of reference 9 (chapter 6) where the momentum theory is applicable. For forward flight ( $\mu>0$ ;  $\sin \beta_i=\pm 1$ ), the same curves apply if the axial component of velocity is used and both coordinate parameters are modified with the  $\sqrt{1+(\mu/\lambda)^2}$  term. Therefore, it will be assumed that the empirical portion of the curve of figure 8 of reference 9 (chapter 6) would also be applicable to forward flight if the  $\sqrt{1+(\mu/\lambda)^2}$  term is included in the coordinate parameters and the axial component of velocity is used. However, the more extensive data of reference 10, modified somewhat in accordance with flight experience such as that reported in reference 8, are used instead.

In figure 2 is plotted the relation between

$$\left(\frac{\lambda}{\sqrt{\frac{C_T}{2B^2\sqrt{1+(\mu/\lambda)^2}}}}\right)_t \quad \text{and} \quad \left(\frac{V \sin \beta/\Omega R}{\sqrt{\frac{C_T}{2B^2\sqrt{1+(\mu/\lambda)^2}}}}\right)_t$$

The regions where the momentum concept is applicable were obtained from equations (A10) and (A11). The vortex region which, as discussed previously, is between  $\left(\frac{V \sin \beta/\Omega R}{\lambda}\right)_t = -0.4$  and  $-2$ , is shown dashed, and is based on figure 12 of reference 10, modified somewhat in

accordance with flight experience, such as that reported in reference 8. By using equation (A1) and the empirical region of figure 2, values of  $\theta_{3BR}$  can be computed for the vortex region for given values of  $(V \sin \beta / \Omega R)_t$ ,  $(C_T / \sigma)_t$ , and  $\left(\frac{\sigma}{\sqrt{1 + (\mu/\lambda)^2}}\right)_t$ .

With the aid of equation (A3), the limits of the vortex region can be expressed in terms of these parameters, for downward inflow, as

$$\left(\frac{V \sin \beta}{\Omega R}\right)_t = -0.24 \left(\sqrt{\frac{C_T}{\sigma}}\right)_t \left(\frac{\sigma}{\sqrt{1 + (\mu/\lambda)^2}}\right)_t \quad (A12)$$

and, for upward inflow, as

$$\left(\frac{V \sin \beta}{\Omega R}\right)_t = -1.46 \left(\sqrt{\frac{C_T}{\sigma}}\right)_t \left(\frac{\sigma}{\sqrt{1 + (\mu/\lambda)^2}}\right)_t \quad (A13)$$

#### DETERMINATION OF $\sqrt{1 + (\mu/\lambda)^2}$

The pitch angle  $\theta_{3BR}$  has thus far been determined as a function of three parameters,  $C_T / \sigma$ ,  $\frac{V \sin \beta}{\Omega R}$ , and  $\frac{\sigma}{\sqrt{1 + (\mu/\lambda)^2}}$ . All of these quantities can normally be easily obtained except  $\sqrt{1 + (\mu/\lambda)^2}$ . The procedure for obtaining  $\sqrt{1 + (\mu/\lambda)^2}$  is now discussed.

The quantity  $\mu/\lambda$  can be obtained by rewriting equation (A2) as follows:

$$\frac{\lambda}{\mu} = \tan \alpha - \frac{1}{\frac{(V/\Omega R)_t^2}{C_T/2B^2} \cos^2 \alpha |\lambda/\mu| \sqrt{1 + (\mu/\lambda)^2}} \quad (A14)$$

For negative values of  $\lambda$ , using the relation  $\beta_t = -\alpha$ , equation (A14) can be solved to give the following equation:

$$\left(\frac{\mu}{\lambda}\right)_t = \left( -\frac{\tan \beta}{2} - \sqrt{\frac{\tan^2 \beta}{4} + \frac{1}{\left[ \frac{(V/\Omega R)^2 \cos^2 \beta}{C_T/2B^2} \sqrt{1 + (\mu/\lambda)^2} \right]}} \right)_t \quad (A15)$$

For positive values of  $\lambda$ , solution of equation (A14) gives

$$\left(\frac{\mu}{\lambda}\right)_t = \left( -\frac{\tan \beta}{2} + \sqrt{\frac{\tan^2 \beta}{4} - \frac{1}{\frac{(V/\Omega R)^2 \cos^2 \beta}{C_T/2B^2} \sqrt{1 + (\mu/\lambda)^2}}} \right)_t \quad (A16)$$

Equations (A15) and (A16) can be used to solve for  $\sqrt{1 + (\mu/\lambda)^2}$  by iteration when fixed values of  $\frac{V/\Omega R}{\sqrt{C_T/2B^2}}$  and  $\beta$  are given.

For the vortex region where the momentum theory is inapplicable, the following empirical procedure is used:

$$\frac{\mu}{\lambda} = \frac{V \cos \alpha / \Omega R}{\lambda} = \frac{\frac{V \sin \alpha / \Omega R}{\sqrt{\frac{C_T}{2B^2 \sqrt{1 + (\mu/\lambda)^2}}}}}{\left( \frac{\lambda}{\sqrt{\frac{C_T}{2B^2 \sqrt{1 + (\mu/\lambda)^2}}}} \right) \tan \alpha}$$

Then, inasmuch as  $\beta_t = -\alpha$ ,

$$\left(\frac{\mu}{\lambda}\right)_t = \left[ \frac{\frac{V \sin \beta / \Omega R}{\sqrt{\frac{C_T}{2B^2 \sqrt{1 + (\mu/\lambda)^2}}}}}{\left( \frac{\lambda}{\sqrt{\frac{C_T}{2B^2 \sqrt{1 + (\mu/\lambda)^2}}}} \right) \tan \beta} \right]_t \quad (A17)$$

By using figure 2, equation (A17) can be solved for  $\sqrt{1 + (\mu/\lambda)^2}$  in the vortex region by iteration when fixed values of  $\left(\frac{V/\Omega R}{\sqrt{C_T/2B^2}}\right)_t$  and  $\beta_t$  are given.

The limits of the vortex region for these parameters can be computed to be, for downward inflow,

$$\left(\frac{V/\Omega R}{\sqrt{C_T/2B^2}}\right)_t = \left(\frac{0.34}{\sqrt{1 + (0.403/\tan \beta)^2 \sin \beta}}\right)_t \quad (A18)$$

and, for upward inflow,

$$\left(\frac{V/\Omega R}{\sqrt{C_T/2B^2}}\right)_t = \left(\frac{2}{\sqrt{1 + (2/\tan \beta)^2 \sin \beta}}\right)_t \quad (A19)$$

## APPENDIX B

### THEORETICAL DEVELOPMENT—RESPONSE TO PEDAL DEFLECTION

The equation for the yaw of the helicopter following a step displacement of the pedals, together with formulas for the stability derivatives required by the solution, are derived in this appendix.

#### EQUATION OF MOTION

By assuming a one-degree-of-freedom system, the equation of motion of a helicopter in yaw is

$$I_z \frac{\partial^2 \eta}{\partial t^2} - \frac{\partial N}{\partial r} \frac{\partial \eta}{\partial t} - \frac{\partial N}{\partial \eta} \Delta \eta = \frac{\partial N}{\partial \theta_t} \Delta \theta_t \quad (B1)$$

The equation of motion is solved by means of the Laplace transformation for a step deflection of  $\Delta \theta_t$  and  $\frac{\partial \eta}{\partial t}(0) = \Delta \eta(0) = 0$ . Using the procedure and tables of reference 11 and converting  $\eta$  to degrees gives

$$\eta(t) = \frac{\left[ e^{at} \left( \frac{a}{b} \sin bt - \cos bt \right) + 1 \right] \frac{\partial N}{\partial \theta_t} \Delta \theta_t \times 57.3}{(a^2 + b^2) I_z} \quad (B2)$$

where  $a \pm bi$  are the roots of the characteristic equation

$$s^2 - \frac{\partial \eta / \partial r}{I_z} s - \frac{\partial N / \partial \eta}{I_z} = 0 \quad (B3)$$

For the special case of  $\frac{\partial N}{\partial \eta} = 0$ , equation (B2) becomes

$$\eta = \frac{e^{ct} - ct - 1}{c^2} \frac{\partial N}{\partial \theta_t} \Delta \theta_t \times 57.3 \quad (B4)$$

where

$$c = \frac{\partial N / \partial r}{I_z} \quad (B5)$$

#### STABILITY DERIVATIVES

During a yawing maneuver, the rotor speed would vary some as a result of the change in rotor torque. In order to simplify the situation to a one-degree-of-freedom system, two extreme cases are studied. In the first case, the rotor speed is assumed to remain constant; whereas, in the second case, the rotor speed is assumed to vary enough that it remains constant with respect to earth axes—that is,  $\Delta \Omega = r$ . In the first case, the main rotor contributes inertia and damping in yaw. In the second case, the resulting change in tail-rotor speed varies the damping in yaw of the tail rotor.

**Assumption of constant rotor speed.**—The equation for the  $\partial N / \partial \theta_t$  derivative is

$$\frac{\Delta N}{\Delta \theta_t} = -l_t \rho (\pi R^2)_t (\Omega R)_t^2 \sigma_t \left( \frac{\Delta C_{T/\sigma}}{\Delta \theta} \right)_t \quad (B6)$$

Changes in tail-rotor thrust due to yawing velocity are, in

general, due to the resultant changes in  $\left( \frac{V \sin \beta}{\Omega R} \right)_t$  and in  $\left( \frac{\sigma}{\sqrt{1 + (\mu/\lambda)^2}} \right)_t$ . Thus, the equation for the  $(\partial N / \partial r)_t$  derivative is

$$\left( \frac{\partial N}{\partial r} \right)_t = \rho [\sigma l_t \pi R^2 (\Omega R)_t^2]_t \left[ \frac{\partial (C_{T/\sigma})_t}{\partial \left( \frac{V \sin \beta - lr}{\Omega R} \right)_t} \frac{\partial \left( \frac{V \sin \beta - lr}{\Omega R} \right)_t}{\partial r} + \frac{\partial (C_{T/\sigma})_t}{\partial \left( \frac{\sigma}{\sqrt{1 + (\mu/\lambda)^2}} \right)_t} \frac{\partial \left( \frac{\sigma}{\sqrt{1 + (\mu/\lambda)^2}} \right)_t}{\partial \beta_t} \frac{\partial \beta_t}{\partial r} \right] \quad (B7)$$

The forward velocity  $V$  and the sideslip angle  $\beta$  at the tail rotor are different from the corresponding values at the helicopter center of gravity if a yawing velocity  $r$  is present.

From a study of figure 10,  $\beta_t$  can be expressed in terms of  $\beta$  and  $r$ ; and  $V_t$  can be expressed in terms of  $V$ ,  $\beta$ , and  $\beta_t$  as follows:

$$\beta_t = \tan^{-1} \left( \tan \beta - \frac{rl_t}{V \cos \beta} \right) \quad (B8)$$

$$V_t = \frac{V \cos \beta}{\cos \beta_t} \quad (B9)$$

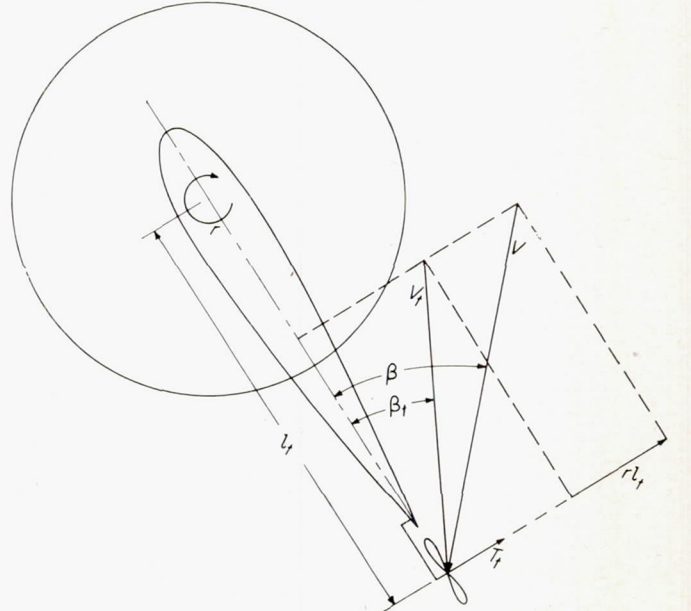


FIGURE 10.—Sketch showing geometry for converting from  $V$ ,  $\beta$ , and  $r$  to  $V_t$  and  $\beta_t$ .  $\tan \beta_t = \frac{V \sin \beta - rl_t}{V \cos \beta} = \tan \beta - \frac{rl_t}{V \cos \beta}$ ;  $V_t = \frac{V \cos \beta}{\cos \beta_t}$ ;  $V_t \sin \beta_t = V \sin \beta - rl_t$ .

Also, the axial component of velocity can be expressed in terms of  $V$ ,  $\beta$ , and  $r$  as

$$V_t \sin \beta_t = V \sin \beta - l_t r \quad (\text{B10})$$

By using equations (B8), (B9), and (B10), and carrying out the indicated differentiations, equation (B7) becomes

$$\left(\frac{\partial N}{\partial r}\right)_t = -\rho[\sigma l(\Omega R)^2 \pi R^2]_t \left[ \frac{\partial(C_T/\sigma)_t}{\partial\left(\frac{V \sin \beta}{\Omega R}\right)_t} \left(-\frac{l}{\Omega R}\right)_t - \left(\frac{l \cos \beta}{V}\right)_t \frac{\partial(C_T/\sigma)_t}{\partial\left(\frac{\sigma}{\sqrt{1+(\mu/\lambda)^2}}\right)_t} \sigma_t \frac{\partial\left(\frac{1}{\sqrt{1+(\mu/\lambda)^2}}\right)_t}{\partial\beta_t} \right] \quad (\text{B11})$$

If constant torque coefficient is assumed, the  $(\partial N/\partial r)_m$  derivative becomes

$$\begin{aligned} \left(\frac{\partial N}{\partial r}\right)_m &= \frac{\partial Q}{\partial r} = -\frac{\partial Q}{\partial \Omega} = -2C_Q \pi R^2 \rho \Omega R^3 \\ &= -\frac{2Q}{\Omega} \end{aligned} \quad (\text{B12})$$

The tail rotor contributes to the directional-stability derivative  $\partial N/\partial \beta$  while the helicopter is hovering in a wind. The contribution can be computed as follows ( $\beta_t$  is assumed equal to  $\beta$  inasmuch as the effect of a yawing velocity is accounted for in the derivative  $(\partial N/\partial r)_t$ ):

$$\begin{aligned} \frac{\partial N}{\partial \beta} &= \frac{\partial N}{\partial \left[\frac{V \sin \beta - l_t r}{(\Omega R)_t}\right]} \frac{\partial \left[\frac{V \sin \beta - l_t r}{(\Omega R)_t}\right]}{\partial \beta} + \\ &\quad \frac{\partial N}{\partial \left(\frac{\sigma}{\sqrt{1+(\mu/\lambda)^2}}\right)_t} \frac{\partial \left(\frac{\sigma}{\sqrt{1+(\mu/\lambda)^2}}\right)_t}{\partial \beta_t} \end{aligned} \quad (\text{B13})$$

Using equation (B10) and carrying out the indicated differentiation gives

$$\begin{aligned} \frac{\partial N}{\partial \beta} &= \frac{\partial N}{\partial \left(\frac{V \sin \beta}{\Omega R}\right)_t} \left[\frac{V \cos \beta}{\Omega R}\right]_t + \\ &\quad \frac{\partial N}{\partial \left(\frac{\sigma}{\sqrt{1+(\mu/\lambda)^2}}\right)_t} \frac{\sigma_t \partial \left(\frac{1}{\sqrt{1+(\mu/\lambda)^2}}\right)_t}{\partial \beta_t} \end{aligned}$$

which may be expressed in terms of the thrust-coefficient—

solidity ratio as follows:

$$\begin{aligned} \frac{\partial N}{\partial \beta} &= -\frac{\partial(C_T/\sigma)_t \sigma_t \rho (\pi R^2)_t (\Omega R)_t^2 l_t \left[\frac{V \cos \beta}{(\Omega R)_t}\right]}{\partial \left(\frac{V \sin \beta}{\Omega R}\right)_t} - \\ &\quad \frac{\partial(C_T/\sigma)_t}{\partial \left(\frac{\sigma}{\sqrt{1+(\mu/\lambda)^2}}\right)_t} (\sigma_t)^2 \rho (\pi R^2)_t (\Omega R)_t^2 l_t \frac{\partial \left(\frac{1}{\sqrt{1+(\mu/\lambda)^2}}\right)_t}{\partial \beta_t} \end{aligned} \quad (\text{B14})$$

**Assumption of  $\Delta\Omega=r$ .**—The additional damping in yaw of the tail rotor due to a variation in tip speed is computed as follows:

$$\Delta \left(\frac{\partial N}{\partial r}\right)_t = -l_t \Delta \left(\frac{\partial T}{\partial r}\right)_t \quad (\text{B15})$$

Inasmuch as  $T_t = C_T \rho (\pi R^2)_t (\Omega R)_t^2$ ,

$$\Delta \left(\frac{\partial N}{\partial r}\right)_t = -l_t \left[ \Delta \frac{\partial(C_T/\sigma)_t}{\partial r} \rho (\pi R^2)_t (\Omega R)_t^2 \sigma_t + \frac{2T_t}{\Omega_t} \frac{\partial \Omega_t}{\partial r} \right] \quad (\text{B16})$$

but, inasmuch as  $\Delta\Omega=r$ , then

$$\frac{\partial \Omega_t}{\partial r} = \frac{\partial \Omega_t}{\partial \Omega} = \frac{\Omega_t}{\Omega} \quad (\text{B17})$$

Also,

$$\Delta \frac{\partial(C_T/\sigma)_t}{\partial r} = \frac{\partial(C_T/\sigma)_t}{\partial \left(\frac{V \sin \beta}{\Omega R}\right)_t} \frac{\partial \left(\frac{V \sin \beta}{\Omega R}\right)_t}{\partial \Omega_t} \frac{\partial \Omega_t}{\partial r} \quad (\text{B18})$$

Carrying out the differentiation,

$$\Delta \left(\frac{\partial C_T/\sigma}{\partial r}\right)_t = \frac{\partial(C_T/\sigma)_t}{\partial \left(\frac{V \sin \beta}{\Omega R}\right)_t} \left(-\frac{1}{\Omega} \frac{V \sin \beta}{\Omega R}\right)_t \frac{\partial \Omega_t}{\partial r} \quad (\text{B19})$$

Substituting equations (B17) and (B19) into equation (B16) gives

$$\Delta \left(\frac{\partial N}{\partial r}\right)_t = -l_t \left[ -\frac{\partial(C_T/\sigma)_t}{\partial \left(\frac{V \sin \beta}{\Omega R}\right)_t} \left(\frac{V \sin \beta}{\Omega R}\right)_t \frac{\sigma_t \rho (\pi R^2)_t (\Omega R)_t^2}{\Omega} + \frac{2}{\Omega} T_t \right] \quad (\text{B20})$$

At trim in unyawed flight,  $(V \sin \beta)_t = 0$ , and equation (B20) becomes

$$\Delta \left(\frac{\partial N}{\partial r}\right)_t = -l_t \frac{2}{\Omega} T_t = -\frac{2Q}{\Omega} \quad (\text{B21})$$

which is identical to equation (B12). Thus, it is seen that, when  $(V \sin \beta)_t = 0$ , the damping-in-yaw contribution of the main rotor computed with the assumption of constant rotor speed is equal to the additional damping-in-yaw contribution of the tail rotor computed with the assumption that  $\Delta\Omega=r$ .

## REFERENCES

1. Anon.: Military Specification; Helicopter Flying Qualities, Requirements for. Military Specification, MIL-H-8501, Nov. 5, 1952.
2. Amer, Kenneth B., and Gustafson, F. B.: Charts for Estimation of Longitudinal-Stability Derivatives for a Helicopter Rotor in Forward Flight. NACA TN 2309, 1951.
3. Wheatley, John B.: An Aerodynamic Analysis of the Autogiro Rotor With a Comparison Between Calculated and Experimental Results. NACA Rep. 487, 1934.
4. Bailey, F. J., Jr.: A Simplified Theoretical Method of Determining the Characteristics of a Lifting Rotor in Forward Flight. NACA Rep. 716, 1941.
5. Gustafson, F. B., and Gessow, Alfred: Effect of Rotor-Tip Speed on Helicopter Hovering Performance and Maximum Forward Speed. NACA WR L-97, 1946. (Formerly NACA ARR L6A16.)
6. Gessow, Alfred: Effect of Rotor-Blade Twist and Plan-Form Taper on Helicopter Hovering Performance. NACA TN 1542, 1948.
7. Carpenter, Paul J.: Effect of Wind Velocity on Performance of Helicopter Rotors As Investigated With the Langley Helicopter Apparatus. NACA TN 1698, 1948.
8. Reeder, John P., and Gustafson, F. B.: On the Flying Qualities of Helicopters. NACA TN 1799, 1949.
9. Gessow, Alfred, and Myers, Garry C., Jr.: Aerodynamics of the Helicopter. The Macmillan Co., c. 1952.
10. Castles, Walter, Jr., and Gray, Robin B.: Empirical Relation Between Induced Velocity, Thrust, and Rate of Descent of a Helicopter Rotor As Determined by Wind-Tunnel Tests on Four Model Rotors. NACA TN 2474, 1951.
11. Churchill, Ruel V.: Modern Operational Mathematics in Engineering. McGraw-Hill Book Co., Inc., 1944.